TOPICAL REVIEW

Micromagnetic modelling—the current state of the art

Josef Fidler and Thomas Schrefl

Institute of Applied and Technical Physics, Vienna University of Technology,
Wiedner Hauptstr. 8-10/137, A-1040 Vienna, Austria

E-mail: `fidler@tuwien.ac.at`

Abstract. The increasing information density in magnetic recording, the miniaturization in magnetic sensor technology, the trend towards nanocrystalline magnetic materials and the improved availability of large-scale computer power are the main reasons why micromagnetic modelling has been developing extremely rapidly. Computational micromagnetism leads to a deeper understanding of hysteresis effects by visualization of the magnetization reversal process. Recent advances in numerical simulation techniques are reviewed. Higher order finite elements and adaptive meshing have been introduced, in order to reduce the discretization error. The use of a hybrid boundary/finite element method enables accurate stray field computation for arbitrary shaped particles and takes into account the granular microstructure of the material. A dynamic micromagnetic code based on the Gilbert equation of motion to study the time evolution of the magnetization has been developed. Finite element models for different materials and magnet shapes are obtained from a Voronoi construction and subsequent meshing of the polyhedral regions. Adaptive refinement and coarsening of the finite element mesh guarantees accurate solutions near magnetic inhomogeneities or domain walls, while keeping the number of elements small. The polycrystalline microstructure and assumed random magnetocrystalline anisotropy of elongated Co elements decreases the coercive field and the switching time compared to zero anisotropy elements, in which vortices form and move only after a certain waiting time after the application of a reversed field close to the coercive field. NiFe elements with flat, rounded and slanted ends show different hysteresis properties and switching dynamics. Micromagnetic simulations show that the magnetic properties of intergranular regions in nucleation-controlled Nd–Fe–B hard magnetic materials control the coercive field. Exchange interactions between neighbouring soft and hard grains lead to remanence enhancement of isotropically oriented grains in nanocrystalline composite magnets. Upper limits of the coercive field of pinning-controlled Sm–Co magnets for high-temperature applications are predicted from the micromagnetic calculations. Incorporating thermally activated magnetization reversal and micromagnetics we found complex magnetization reversal mechanisms for small spherical magnetic particles. The magnetocrystalline anisotropy and the external field strength determine the switching mechanism. Three different regimes have been identified. For fields, which are smaller than the anisotropy field, magnetization by coherent switching has been observed. Single droplet nucleation occurs, if the external field is comparable to the anisotropy field, and multi-droplet nucleation is the driving reversal process for higher fields.

1. Introduction

The micromagnetic theory is an approach to explain the magnetization reversal or hysteresis effects of ferro- and ferrimagnetic materials at an intermediate length scale between magnetic domains and crystal lattice sites. Originally in micromagnetics (Brown 1963a) a continuous magnetization vector is used to describe the details of the transition region between magnetic domains (Landau 1935) instead of taking account of the individual atomic moments. Micromagnetism is a generic term used for a wide variety of studies of magnetization structures and reversal mechanisms in magnetic materials. Since the

mid 1980s the improved availability of large-scale computer power has enabled the study of increasingly detailed and subtle physical behaviour, which has also impacted on the rapid technological development of advanced magnetic materials. The increasing impact of magnetic materials on many modern industries will continue well into this century. Besides recording materials and soft magnetic devices, also hard magnetic materials are key components in information and transportation technologies, machines, sensors and many other systems. Over the past few years micromagnetism has been developing extremely rapidly for several reasons. Modern soft and hard magnetic materials and recording media consist of nanocrystalline

grains with grain sizes less than 50 nm. Nanofabrication, offering unprecedented capabilities in the manipulation of material structures and properties, opens up new opportunities for engineering innovative magnetic materials and devices, developing ultra-high-density magnetic storage. The reduced grain size considerably increases the storage density of high-density magneto-optical and longitudinal recording media (Weller 1999, Richter 1999). Nanoscale Ni–Fe and Co patterned media are able to achieve recording densities higher than 100 Gbits inch^{-2} (Chou 1997). Numerical micromagnetic modelling using the finite difference or finite element method reveals the correlation between the local arrangement of the magnetic moments and the microstructural features on a length scale of several nanometres. Computational micromagnetics gives a quantitative treatment of the influence of the microstructure and shape of the magnet device on the magnetization reversal and hysteresis processes.

Traditional investigations of magnetization reversal in small ferromagnetic particles assume spherical or ellipsoidal particles uniformly magnetized along the easy direction for zero applied field. At the nucleation field the magnetization starts to deviate from the equilibrium state according to the preferred magnetization mode (Frei 1957, Aharoni 1962). The magnetization reversal mechanism in nonellipsoidal particles has been rigorously studied applying finite difference (Schabes 1988, Nakatani 1989) or finite element techniques (Koehler 1992). The numerical results clearly show that strong stray fields, which cause the magnetization to become inhomogeneously arranged, influence the reversal process drastically (Victora 1988, Yan 1988, Schabes 1991). Owing to stray field effects the angular dependence of the nucleation field of nonellipsoidal particles considerably deviates from the classical results (Schmidts 1992). In addition to the self-demagnetizing field of polyhedral particles, exchange and magnetostatic interactions between the grains lead to inhomogeneous magnetic states. Consequently interparticle interactions affect the magnetic properties of ferromagnetic materials. Spratt et al (1991) reported a reduced nucleation field of two interacting cubic particles owing to magnetostatic interactions. Fukunaga and Inoue (1992) investigated the effects of intergrain exchange and magnetostatic interactions on remanence and coercivity for an isotropic model magnet composed of cubic particles. The results show that intergrain exchange interactions increase the remanence and reduce the coercive field of isotropic permanent magnets. To investigate the effects of long-range magnetostatic interactions in sintered permanent magnets, simplified numerical models have been developed (Ramesh 1988, Blank 1991, Gabay 1992). These models take correctly into account the interactions between the particles, but derive the nucleation field of the individual particles by fitting the numerically calculated demagnetization curves to experimental hysteresis loops. Thus, these models favourably describe collective effects on the demagnetization curve, whereas they neglect the microstructural origins, which determine the nucleation field. Hernando et al (1992) presented a one-dimensional micromagnetic model for investigating intergrain exchange interactions in hard magnetic materials. The formation

of a domain-wall like magnetization distribution at the interface between neighbouring grains with different orientation reduces the nucleation field drastically. Zhu and Bertram (1988) studied interparticle interactions in thin-film recording media represented by a two-dimensional array of hexagonal grains. Decreasing the effective exchange coupling between the grains enhances coercivity and reduces coercive squareness. Long-range magnetostatic interactions correlate the magnetization over several grains resulting in magnetic clustering. New numerical procedures were developed describing the dynamical behaviour by the finite element method in three-dimensional micromagnetic systems by Yang and Fredkin (1998). Modelling the thin-film microstructure by randomly located ellipsoidal particles, Miles and Middleton (1990) showed that the spatial arrangement of the grains affects the hysteresis properties owing to magnetostatic interactions. Micromagnetic models have been used to derive the recording properties of dual-layer thin-film recording media (Zhu 1992, Oti 1993). Vos et al (1993) developed a micromagnetic model to investigate interaction effects in particulate recording media. The numerical results obtained for an assembly of ellipsoidal particles show that the interplay between particle shape and magnetostatic interactions significantly affects coercivity and coercive squareness. Nanocrystalline ferromagnets show excellent soft magnetic properties. As the grain size becomes smaller than the ferromagnetic exchange length, exchange interactions between the grains suppress the magnetocrystalline anisotropy of the individual particles. With decreasing grain size coercivity steeply decreases, varying with the sixth power of the grain size (Herzer 1990). The random anisotropy model (Alben 1978) can be successfully applied to describe the grain size dependence of coercivity and initial permeability in nanocrystalline ferromagnets. Whereas the random anisotropy model completely neglects microstructural features, Navarro et al (1993) investigated the role of intergrain exchange coupling between magnetically hard and soft phases in nanocrystalline ferromagnets.

A large number of scientific papers concentrate nowadays on such areas as (i) how to incorporate thermally activated magnetization reversal in the framework of the micromagnetic concept (Boerner 1997, Chantrell 1998, Lyberatos 1993, Nakatani 1997, Zhang 1999), (ii) how to simulate the influence of complex microstructures on the magnetization reversal and to expand the theory to new techniques for the simulation of large-scale systems, such as magnetic storage devices, sensors and others. Future activities will concentrate on the development of hybrid micromagnetic models including Monte Carlo approaches (Hinzke 1999, Nowak 2000).

We developed a new numerical procedure to study static and dynamic behaviour in micromagnetic systems. This procedure solves the damped Gilbert equation for a continuous magnetic medium, including all interactions in standard micromagnetic theory in three-dimensional regions of arbitrary geometry, polycrystalline grain structure and physical properties. Sections 2–5 of the paper give the micromagnetic background and the computational details. This paper reviews recent advances in numerical

micromagnetic 3D simulations and shows how our numerical micromagnetic code has been used to solve actual problems in novel magnetic materials and devices. This code has been successfully applied to various problems, such as switching dynamics of magnetic NiFe and Co elements (Schrefl 1997a, c) remanence enhancement in exchange-coupled, nanocrystalline $(Nd_2Fe_{14}B)_x(Fe_3B/\alpha\text{-}Fe)_{1-x}$ hard magnets (Schrefl 1998, 1999b), the nucleation field of high energy density $Nd_2Fe_{14}B$ magnets (Suess 2000), the domain wall pinning in high-temperature $Sm(Co, Fe, Cu, Zr)_{7-8}$ magnets (Streibl 2000), the thermal activation and switching field of small Co particles (Scholz 2000) and the incorporation of the method of adaptive mesh refinement (Scholz 1999). Sections 6–8 present the numerical results focusing on the interaction between microstructural features and the magnetization reversal processes.

2. Micromagnetic equations

Micromagnetism is essentially a continuum approximation which allows the calculation of magnetization structures and magnetization reversal assuming the magnetization to be a continuous function of position, and deriving relevant expressions for the important contribution arising from the exchange, magnetostatic and anisotropy energies. Minimizing the total Gibb's free energy with respect to the magnetization yields a stable equilibrium state of the magnetic structure. All energy terms but the stray field energy depend only locally on the magnetization. Thus the direct evaluation of the total magnetic Gibb's free energy requires both large memory space and long computation time. The magnetostatic field is a long-range interaction whose calculation is the most time-consuming part of the micromagnetic problem. Introducing a magnetic vector potential to treat the demagnetizing field eliminates long-range interactions from the total magnetic Gibb's free energy (Asselin 1986, Aharoni 1991). This leads to a sparse, algebraic minimization problem. Since the magnetic polarization J and the magnetic vector potential A are independent variables, the minimization can be performed simultaneously with respect to J and A. Alternatively, it is possible to introduce a magnetic scalar potential Ψ to compute the demagnetizing field. The energy functional is free from any long-range term leading to effective numerical algorithms that require only limited memory.

Starting from the vector of the magnetic polarization as a function of space and time
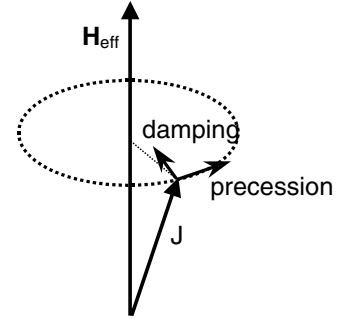
$$J(r, t) = J_s \cdot u(r, t) \qquad \sum u_i^2 = 1 \qquad (1)$$

leads to a standard total free energy expression for a system within a certain volume:

$$E_t(J, A) = \int \left[\frac{A}{J_s^2} (\nabla J)^2 - K_1 \left(u_c \cdot \frac{J}{J_s} \right)^2 \right.$$
$$\left. - J \cdot H_{ext} + \frac{1}{2\mu_0} (\nabla \times A - J)^2 \right] dV \qquad (2)$$

or

$$E_t(J, \Psi) = \int \left[\frac{A}{J_s^2} (\nabla J)^2 \right.$$
$$\left. - K_1 \left(u_c \cdot \frac{J}{J_s} \right)^2 - J \cdot H_{ext} - J \cdot \nabla \Psi \right] dV \qquad (3)$$

Figure 1. Damped gyromagnetic precession motion of a single magnetic polarization vector J towards the effective magnetic field H_{eff} according to the Gilbert equation of motion.

with the constraint

$$\Delta \Psi = -\frac{1}{\mu_0} \nabla J. \qquad (4)$$

The temperature dependent constants J_s, A, K_1 are the saturation polarization, the exchange constant and the magnetocrystalline anisotropy constant, respectively. The first term of the total energy expression is the exchange energy, followed by the magnetocrystalline anisotropy energy for uniaxial systems with the easy axis direction u_c, the Zeeman coupling to an external magnetic field H_{ext} and the stray field energy arising from magnetic dipole interactions. The last term is the most severe problem to be solved. In order to save computation time the demagnetizing field is sometimes solved analytically. Because of this problem there is also a tendency to utilize extremely simplified, regular microstructures whose periodicity can be used to speed up the magnetic field calculations, but which can be shown to introduce unwanted artefacts into the computational results. The direct computation of the demagnetizing field from the magnetic volume and surface charges (Aharoni 1996) scales with N^2 in storage and computation time, where N denotes the number of grid points in a finite different or finite element discretization of the magnetic device. Fast adaptive algorithms have been applied in numerical micromagnetics using FFT or multipole expansion on regular computational grids (Yuan 1992), in order to speed up the calculations. Finite element based micromagnetic codes effectively treat the microstructure of the system, including the shape of the magnet and the irregular grain structure (Schrefl 1999a). The FFT method cannot be applied on the corresponding unstructured mesh, such as in finite element field calculation, where micromagnetic finite element simulations introduce a magnetic scalar or magnetic vector potential to calculate the demagnetizing field (Schrefl 1999a). Fredkin and Koehler (1990) proposed a hybrid finite element (FE)/boundary element (BE) method to treat the open boundary problem associated with calculation of the magnetic scalar potential. This method is accurate and allows the calculation of the magnetostatic interaction between distinct magnetic elements without any mesh between the magnetic particles. However, the conventional boundary element method requires storage of a dense matrix.

From the thermodynamical principle of irreversibility, the equation of motion for the magnetic polarization was derived by Landau and Lifshitz (1935)

$$\frac{\partial \boldsymbol{J}}{\partial t} = -\frac{|\gamma|}{1+\alpha^2}(\boldsymbol{J} \times \boldsymbol{H}_{eff}) - \frac{\alpha}{J_s(1+\alpha^2)}[\boldsymbol{J} \times (\boldsymbol{J} \times \boldsymbol{H}_{eff})]$$

(5)

with

$$\boldsymbol{H}_{eff} = -\frac{\delta E_t}{\delta \boldsymbol{J}}$$

(6)

or in the equivalent form given by Gilbert (1955)

$$\frac{\partial \boldsymbol{J}}{\partial t} = -|\gamma|(\boldsymbol{J} \times \boldsymbol{H}_{eff}) + \frac{\alpha}{J_s}\left(\boldsymbol{J} \times \frac{\partial \boldsymbol{J}}{\partial t}\right).$$

(7)

In numerical micromagnetics generally the following scheme is used in order to calculate a hysteresis loop. At first the model magnet is saturated applying a high external field. The uniform magnetic state with magnetization pointing parallel to the field direction corresponds to a minimum of the total magnetic Gibb's free energy. The repeated minimization of the energy for decreasing and increasing the applied field provides the hysteresis curve. A small change in the external fields alters the energy surface slightly and thus the system is no longer in equilibrium. Unless the change of the external field alters the curvature of the energy surface, the current position of the system will be close to a local minimum of the energy. If the local minimum vanishes as the curvature changes, the system has to find its path towards the next local minimum. Equations (5) and (7) describe the physical path the system follows towards equilibrium (figure 1). The effective field $\boldsymbol{H}_{eff}$, which provides the torque acting on the magnetization, is the negative functional derivative of the total magnetic Gibb's free energy. The first term on the right-hand side of (5) and (7) describes the gyromagnetic precession, where γ is the gyromagnetic ratio of the free electron spin. The second term describes the dissipation of energy. It causes the magnetization to become aligned parallel to the effective field as the system proceeds towards equilibrium; the Gilbert damping parameter α is dimensionless. Alternatively, numerical minimization methods may be used to compute the equilibrium states, which considerably reduce the computational effort as compared to the numerical integration of the Gilbert equation. The dynamic micromagnetic simulation allows one to describe the time evolution of the magnetization, if the damping parameter α is sufficiently known. For common ferromagnetic materials α is not constant and depends nonlinearly on the magnetization. For numerical convenience α is often set to a value between 0.1 and 1, which results in a reduced computation time. Usually the Gilbert damping parameter is determined from the line broadening in ferromagnetic resonance measurements. The deeper understanding of the damping process is rather complex. The origin of magnetic moments is primarily due to the spin of the charge carriers. Only quantum mechanics describes the interactions between the charge carriers with each other. In the phenomenological description of micromagnetics the effect of the microscopic physical processes are accommodated into the single parameter α, which governs the rate of approach to equilibrium and is
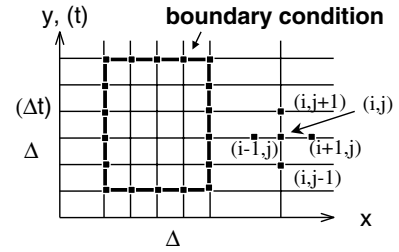
Figure 2. Schematic discretization of a given region in the $(x, y)/(x, t)$ plane, subdivided into FD elements, in which the micromagnetic equations are satisfied.

used to fit the experiment (Inaba 1997). The fact that α has different values under different conditions, and appears to be a function of the magnetization state, indicates that the extent of the contribution from spin–spin interactions, which can be formulated in terms of magnon–magnon scattering processes, plays an important role in determining the value α (Wongsam 2000, Garanin 1997).

3. Micromagnetic concept of the finite difference technique

The finite-differences (FD) method is a widely used numerical method for finding approximate values of solutions of problems involving partial differential equations. The basic idea of the method consists of approximating the partial derivatives of a function $u(\boldsymbol{r}, t)$ by finite difference quotients $\Delta x, \Delta y, \Delta z$ and Δt.

$$u(x + \Delta x, y, z, t) = u(x, y, z, t) + \Delta x \frac{\partial u(x, y, z, t)}{\partial x}$$
$$+ \frac{(\Delta x)^2}{2} \frac{\partial^2 u(x, y, z, t)}{\partial x^2} + \cdots.$$

(8)

The process of replacing partial derivatives by FD quotients is known as a discretization process and the associated error is the discretization error. A partial differential equation can be changed to a system of algebraic equations by replacing the partial derivatives in the differential equation with their FD approximations. The system of algebraic equations can be solved numerically by an iterative process in order to obtain an approximate solution. The FD method is nowadays widely used to solve elliptic, hyperbolic and parabolic equations. Most numerical micromagnetic simulations rely on the finite difference method (Zhu 1995).

Figure 2 schematically shows a given region in the $(x, y)/(x, t)$ plane, subdivided into FD elements, in which the partial differential equation is satisfied. The solution or derivative is specified on the boundary. The approximate solution at the interior grid points is obtained by solving a system of algebraic equations. Replacing both space and time derivatives by their FD approximations, we can solve for the $u(i, j)$ in the difference equation explicitly in terms of the solution at earlier values of time. This process is called an explicit-type marching process. Stable solutions are only obtained in all cases if the chosen time steps are sufficiently small compared to the spatial discretization.

In order to solve numerically the Landau–Lifshitz (5) or Gilbert equation (7) with the effective field (6), we have to convert it into a form which can be translated

into an algorithm for a digital computer with finite speed and memory. We have to reduce the problem of finding a continuous solution to one with finite dimensionality (Grossmann 1994). In the FD method, as later in the FE method, we replace the continuous solution domain by a discrete set of lattice points. In each lattice point we replace any differential operators by FD operators. The conditions on the boundary of the domain have to be replaced by their discrete counterparts. For some differential equations, such as the wave equation in one dimension, it is even possible to construct exact algorithms by non-standard FD schemes (Cole 1998). However, this is rarely the case, and so the finite difference method gives only an approximate solution. For our problem of calculating the effective field and integrating the Landau–Lifshitz or Gilbert equation, we have to discretize time and space into regular lattices. For the space discretization a regular cubic lattice has been chosen, because it allows the simplest implementation and irregular lattices are more efficiently handled with the FE method. The time integration is also done on a regular lattice.

Each computational cell has a magnetic moment $\Delta x \Delta y \Delta z \boldsymbol{J}_i / \mu_0$ which is the product of its volume $\Delta x \Delta y \Delta z$ and the saturation magnetization of the material. The time evolution of the magnetization is obtained by integrating equation (5) or (7) for each computational cell. The local field is calculated after each time step for each computational cell. In order to calculate the contribution of the exchange interaction to the effective field, we have to discretize the first term in equation (2). The final result of the contribution of the discretized exchange energy to the effective field at the lattice site i is

$$H_{exch,i} = \frac{2A}{\Delta x^2 \cdot J_s^2} \sum_{i \in NN} \boldsymbol{J}_i \qquad (9)$$

where NN stands for the indices of the nearest neighbours.

The approximation of the partial derivatives by FDs is only valid for small arguments, and in our case for small angles between neighbouring magnetization vectors. Other exchange energy representations have been suggested and compared (Donahue 1997), but none of them has significant advantages over the one derived above. The contributions by the external field and the magnetocrystalline anisotropy to the effective field are straightforward:

$$H_{ani} = \frac{2K_1}{J_s^2} \boldsymbol{u}_c (\boldsymbol{J} \cdot \boldsymbol{u}_c). \qquad (10)$$

Another difficulty arises from the calculation of the demagnetizing field. Within each computational cell, the Wigner–Seitz cell of the lattice point, the magnetization is assumed to be homogeneous. We could now try to discretize Poisson's equation of the scalar magnetic potential Ψ inside the magnet and Laplace's equation of Ψ outside the magnet. However, for a lattice of homogeneously magnetized cubes, it is possible to calculate the demagnetizing field analytically (Schabes 1987). The expressions obtained are quite complex and computationally expensive to implement. Since the calculation of the demagnetization field by a magnetic scalar potential is very efficiently implemented in the FE package, a third possibility has been chosen for the FD program.

This is the approximation of the demagnetization field of each computational cell by the field of a magnetic dipole in the centre of the cell with the magnetic moment $\Delta x^3 \boldsymbol{J}_i / \mu_0$ (Opheusden 1990, Boerner 1997).

$$\boldsymbol{H}_{dip} = -\frac{\Delta x^3}{\mu_0 4\pi} \sum_{j \neq i} \left(\frac{\boldsymbol{J}_j}{R_{ij}^3} - 3\frac{\boldsymbol{R}_{ij}(\boldsymbol{J}_j \cdot \boldsymbol{R}_{ij})}{R_{ij}^5} \right). \qquad (11)$$

The inaccuracy is not large and the true long-range nature of the problem is kept (Aharoni 1991). This is due to the fact, that the quadrupole moment of a uniformly magnetized cube is identically zero. Only the next term in a multipole expansion, the octapole term, would give a nonzero contribution (DellaTorre 1986). Many research groups use the FD method for their micromagnetic simulations. The calculation of the demagnetizing field is often done by more advanced methods based on the analytic solution for homogeneously magnetized hexahedra (Schabes 1987) or fast Fourier transformations (Berkov 1998, Fabian 1996). However, stiff modes cause deteriorating convergence rates (Lewis 1997).

Another problem arises from complicated geometries (possibly with curved boundaries) and irregular microstructures. As the finite difference method requires the use of a regular lattice, it is difficult to handle curved boundaries, because they are always approximated by small steps. Only recently, the 'embedded curved boundary method' succeeded in generating results similar to those of the FE method (Parker 2000, Gibbons 1999). Expect in the case of simple geometries and boundary conditions, it is almost impossible to achieve a direct analytical solution of the micromagnetic differential equations. Numerical methods are generally required to obtain the solution for all but the simplest geometries, but the use of the FD method can become tedious, when modelling complex shapes found in micromagnetic problems.

4. FE techniques in micromagnetics

The FE method has become a well established method in many fields of computer aided engineering, such as structural analysis, fluid dynamics, and electromagnetic field computation. However, its flexibility in modelling arbitrary geometries comes at the cost of a more complex mathematical background. There are three main steps during the solution of a partial differential equation (PDE) with the FE method. First, the domain, on which the PDE should be solved, is discretized into finite elements. Depending on the dimension of the problem these can be triangles, squares, or rectangles in two dimensions or tetrahedrons, cubes, or hexahedra for three-dimensional problems. The solution of the PDE is approximated by piecewise continuous polynomials and the PDE is hereby discretized and split into a finite number of algebraic equations. Thus, the aim is to determine the unknown coefficients of these polynomials in such a way, that the distance (which is defined by the norm in a suitable vector space) from the exact solution becomes a minimum. Therefore, the FE method is essentially a minimization technique for variational problems. Since the number of elements is finite, we have reduced the problem of finding
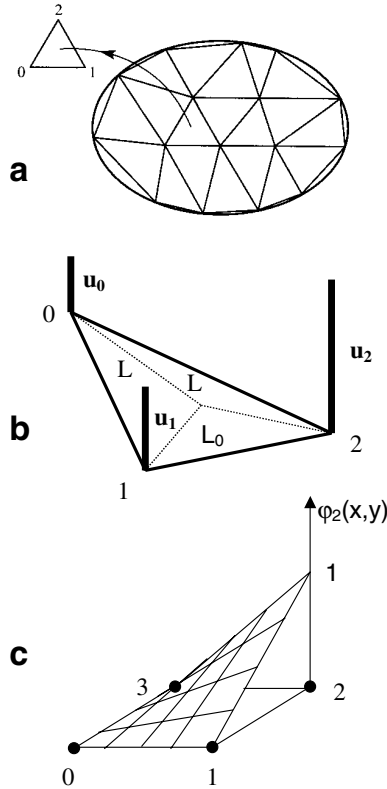
Figure 3. (a) Triangulation of a two-dimensional domain into finite elements. (b) Interpolation using a linear function within a triangular finite element between the nodal points 0, 1 and 2. (c) is an example for the shape function $\varphi_2(x, y)$ for a quadrilateral.

a continuous solution for our PDE to calculating the finite number of coefficients of the polynomials.

The principle of the FE method involves transforming the field equations into an energy functional:

$$I[\boldsymbol{J}, \boldsymbol{A}] = \int F\{J_x(\boldsymbol{r}), J_y(\boldsymbol{r}), J_z(\boldsymbol{r}), A_x(\boldsymbol{r}),$$
$$A_y(\boldsymbol{r}), A_z(\boldsymbol{r}), \Psi(\boldsymbol{r}) \ldots\} \, dV. \tag{12}$$

The functional $I[\boldsymbol{J}, \boldsymbol{A}]$ has a numerical value at each point within a region and is an integral representation throughout the entire field volume of the variables that are functions of the geometry, material properties, the potential solution and its derivatives. The first variation of the energy functional with respect to its variables yields the original PDE of the field. Asselin and Thiele (1986) showed that the first variation of (2) leads to Brown's micromagnetic (Brown 1963a) equations and the equation for the vector potential $\boldsymbol{A}$. A suitable functional will therefore be any expression whose minimum, obtained by differentiation with respect to potential and being set equal to zero, is the field expression. This procedure is performed for each nodal potential at each element in a set of linear algebraic equations which describe the entire region. Under these conditions, the distribution of $\boldsymbol{J}(\boldsymbol{r}, t)$ may be determined from the energy functional rather than from the PDE at the nodal points of the mesh and suitably interpolated within each finite element.

The FE method is a particular Galerkin method, which uses piecewise polynomial functions to construct the finite dimensional subspace. The solution domain is divided into many small subdomains, referred to as finite elements. In two space dimensions these elements are usually triangles (figure 3(a)) or convex quadrilaterals, while in three dimensions tetrahedra, prisms and hexahedra are commonly employed. This subdivision process is usually called triangulation. The collection of all elements is referred to as the FE mesh or grid. The FE solution is initiated by dividing the entire region into elements of various shapes, as shown in figure 3. These element boundaries adapt much more readily to complex geometries than in the case of FD elements.

The value of the potential/function $u(\boldsymbol{r})$ is calculated at N nodal points of the mesh, and the function is interpolated in each element (linear, quadratics, cubics, . . .):

$$u(x, y) = a + b_1 x + c_1 y + b_2 x^2 + c_2 y^2 + \cdots b_3 x^3 + c_3 y^3 + \cdots. \tag{13}$$

Within each element, the potential/function $u(\boldsymbol{r})$ is described in the 2D space according to its nodal values u_i:

$$u(x, y) = \frac{1}{L} \sum_{i=0}^{2} L_i(x, y) u_i. \tag{14}$$

In micromagnetics the magnetic polarization is defined at the nodal points of the FE mesh. The magnetic polarization $\boldsymbol{J}(\boldsymbol{r})$ may be evaluated everywhere within the model magnet, using the piecewise polynomial interpolation of the polarization on the FE mesh. Figure 3(b) illustrates the interpolation using a linear function on a triangular finite element. The polarization in a point r within the element is the weighted average of the magnetization at the nodal points 0, 1 and 2.

$$\boldsymbol{J}(\boldsymbol{r}) = \frac{1}{L_0 + L_1 + L_2} \sum_{i=0}^{2} L_i \boldsymbol{J}(\boldsymbol{r}_i)$$
$$= \frac{1}{L}[L_0 \boldsymbol{J}(\boldsymbol{r}_0) + L_1 \boldsymbol{J}(\boldsymbol{r}_1) + L_2 \boldsymbol{J}(\boldsymbol{r}_2)] = \sum_{i=0}^{2} \varphi_i \boldsymbol{J}(\boldsymbol{r}_i). \tag{15}$$

L denotes the total area of the element and L_i are the areas of the subtriangles. A similar interpolation scheme applies for tetrahedral elements in three dimensions. The function $\varphi_i = L_i/L$ is called a shape function, which equals one on the node i and is zero on all the other nodes of the element (figure 3(c)). The shape function $\varphi_i(\boldsymbol{r})$ satisfies the condition

$$\varphi_i(\boldsymbol{r}_j) = \delta_{ij} \tag{16}$$

where $\boldsymbol{r}_j$ denotes the cartesian coordinates of the nodes $j = 1, \ldots, N$. Figure 3(c) depicts an example for the shape function φ_i.

The FE mesh is used to integrate the total magnetic Gibb's free energy over the magnet. The energy integral is then replaced by a sum over cells (triangles, tetrahedrons, hexahedrons, etc), and (15) is applied to perform the integration of the energy over each cell.

Both static and dynamic micromagnetic FE calculations start from the discretization of the total magnetic Gibb's free energy (2). When $\boldsymbol{J}(\boldsymbol{r})$ is approximated by piecewise polynomial functions on the FE mesh, the energy functional reduces to an energy function with the nodal values of the

polarization, $\boldsymbol{J}_i = (J_{x,i}, J_{y,i}, J_{z,i})$, as unknowns. The total energy may be written as

$$E_t = E_t[\boldsymbol{J}(\boldsymbol{r})] = E_t(J_{x,1}, J_{y,1}, J_{z,1}, J_{x,2}, J_{y,2}, J_{z,2}, \ldots,$$
$$J_{x,N}, J_{y,N}, J_{z,N}) \qquad (17)$$

where N is the total number of nodal points. The minimization of (17) with respect to the $3N$ variables $\boldsymbol{J}_i$ subject to the constraint $|\boldsymbol{J}_i| = \boldsymbol{J}_s$ provides an equilibrium distribution of the polarization. To satisfy the constraint, polar coordinates θ_i, ϕ_i for the polarization at node i may be introduced, such that $J_{x,i} = J_s \sin\theta_i \cos\phi_i$, $J_{y,i} = J_s \sin\theta_i \sin\phi_i$, $J_{z,i} = J_s \cos\theta_i$. An alternative approach (Koehler 1997) is to normalize the magnetization in the discretized energy function (17), replacing $\boldsymbol{J}_i$ by $\boldsymbol{J}_i/J_s$. In both cases, the minimization may be effectively performed using a conjugate gradient method (Gill 1993). Conjugate gradient based minimization techniques require the gradient of the energy to select the search directions. Using polar coordinates, the gradient of the energy can be expressed as

$$\frac{\partial E_t}{\partial \theta_i} = \frac{\partial E_t}{\partial J_{x,i}} \frac{\partial J_{x,i}}{\partial \theta_i} + \frac{\partial E_t}{\partial J_{y,i}} \frac{\partial J_{y,i}}{\partial \theta_i} + \frac{\partial E_t}{\partial J_{z,i}} \frac{\partial J_{z,i}}{\partial \theta_i}$$
$$= -V_i \boldsymbol{H}_{eff,i} \cdot \frac{\partial \boldsymbol{J}_i}{\partial \theta_i} \qquad (18)$$

$$\frac{\partial E_t}{\partial \phi_i} = \frac{\partial E_t}{\partial J_{x,i}} \frac{\partial J_{x,i}}{\partial \phi_i} + \frac{\partial E_t}{\partial J_{y,i}} \frac{\partial J_{y,i}}{\partial \phi_i} + \frac{\partial E_t}{\partial J_{z,i}} \frac{\partial J_{z,i}}{\partial \phi_i}$$
$$= -V_i \boldsymbol{H}_{eff,i} \cdot \frac{\partial \boldsymbol{J}_i}{\partial \phi_i}. \qquad (19)$$

The effective field $\boldsymbol{H}_{eff}$ at the nodal points of the FE mesh is calculated within the framework of the box method. The effective field at nodal point i of the FE mesh is approximated by (Gardiner 1985)

$$\boldsymbol{H}_{eff,i} = -\left(\frac{\delta E_t}{\delta \boldsymbol{J}}\right)_i \approx -\frac{1}{V_i}\frac{\partial E_t}{\partial \boldsymbol{J}_i} \qquad (20)$$

where V_i is the volume of a 'box' surrounding the nodal point i.

Both static and dynamic micromagnetic calculations require evaluation of the effective field (20) at the nodal points of the FE mesh. The effective field is the sum of the exchange field, the anisotropy field, the magnetostatic field, and the external field. The exchange field and the anisotropy field depend only locally on the magnetization or its spatial derivatives and thus may be directly calculated using (20). The magnetostatic field depends on the magnetization distribution over the entire magnet. It arises from the non-zero divergence within the grains ('magnetic volume charges') and the intersection of the magnetization with the grain surface ('magnetic surface charges'). Numerical micromagnetics makes use of the well established methods for the FE calculation of magnetostatic fields (Silvester 1983). The magnetostatic field is either derived from a magnetic scalar or magnetic vector potential. The FE discretization of the corresponding PDE leads to a system of linear equations. Owing to the local character of the equations the corresponding system matrix is symmetric and sparse. State of the art solution techniques for sparse linear systems consist of a preconditioning step, followed by the iterative solution of the linear system using a conjugate gradient based method. For a given FE mesh the preconditioning of the system matrix has to be done only once, reducing the effort for the subsequent calculations of the magnetostatic field to about $N^{1,3}$ (Marsal 1989), where N is the total number of grid points. Thus, the use of the FE method to treat the auxiliary problem for the magnetostatic field provides an alternative fast solution technique without any restriction on the geometry of the magnetic particles.

The magnetostatic contribution to the effective field is the negative gradient of the magnetic scalar potential. The magnetic scalar potential satisfies the Poisson equation

$$\Delta \Psi(\boldsymbol{r}) = \frac{1}{\mu_0} \nabla \cdot \boldsymbol{J}(\boldsymbol{r}). \qquad (21)$$

Outside the magnetic particle $\boldsymbol{J}$ equals zero and thus (21) reduces to the Laplace equation. At the boundary of the magnet r the boundary conditions hold

$$\Psi^{int} = \Psi^{ext} \qquad (\nabla\Psi^{int} - \nabla\Psi^{ext}) \cdot \boldsymbol{n} = \frac{1}{\mu_0} \boldsymbol{J} \cdot \boldsymbol{n}. \quad (22)$$

Here $\boldsymbol{n}$ denotes the outward pointing normal unit vector. The magnetic scalar potential is regular at infinity. The Galerkin method is applied to transfer the magnetostatic boundary value problem to a system of linear equations. The PDE (21) is multiplied by test functions, and integrated over the problem domain. Within the framework of the Galerkin method, the shape functions φ_i, given by (16), are used as test functions.

$$\int \left[\Delta\Psi(\boldsymbol{r}) - \frac{1}{\mu_0}\nabla \cdot \boldsymbol{J}(\boldsymbol{r})\right] \cdot \varphi_i(\boldsymbol{r}) \, \mathrm{d}V = 0. \qquad (23)$$

The test functions φ_i are the basis functions for the expansion of Ψ on the FE mesh.

$$\Psi(\boldsymbol{r}) = \sum_i \varphi_i^e(\boldsymbol{r})\Psi_i = \varphi_i^e(\boldsymbol{r})\Psi_i \qquad (24)$$

where Ψ_i denotes the values of the magnetic scalar potential at the nodes of the element. Integration by parts of (23), inserting the boundary condition (22), and replacing $\Psi(\boldsymbol{r})$ by (24) yields the sparse, linear system of equations that gives the potential Ψ, at nodes i of the FE mesh.

In order to impose the regularity condition, the FE mesh has to be extended over a large region outside the magnetic particles (at least five times the extension of the particle (Chen 1997)). Various other techniques have been proposed to reduce the size of the external mesh or to avoid a discretization of the exterior space. The use of asymptotic boundary conditions (Yang 1998) reduces the size of the external mesh as compared to truncation. At the external boundary, Robbin conditions, which are derived from a series expansion of the solution of the Laplace equation for Ψ outside the magnet and give the decay rate of the potential at a certain distance from the sample, are applied (Khebir 1990). A similar technique that considerably reduces the size of the external mesh is the use of space transformations to evaluate the integral over the exterior space. Among the various transformations proposed to treat the open boundary problem, the parallelepipedic shell transformation (Brunotte 1992), which maps the external space into shells enclosing the parallelepipedic interior

domain, has proved to be most suitable in micromagnetic calculations. The method can be easily incorporated into standard FE programs transforming the derivatives of the nodal shape functions. This method was applied in static three-dimensional micromagnetic simulations of the magnetic properties of nanocrystalline permanent magnets (Schrefl 1998, Fischer 1998a).

An alternative approach to treat the so-called open boundary problem is a hybrid FE/BE method (Fredkin 1990, Koehler 1997). The basic concept of this method is to split the magnetic scalar potential into $\Psi = \Psi_1 + \Psi_2$, where the potential Ψ_1 is assumed to solve a closed boundary value problem. Then the equations for Ψ_2 can be derived from (21)–(22), which hold for the total potential $\Psi = \Psi_1 + \Psi_2$. The potential Ψ_1 accounts for the divergence of the magnetization and Ψ_2 is required to meet the boundary conditions at the surface of the particle. The potential Ψ_1 is the solution of the Poisson equation within the magnetic particles and equals zero outside the magnet. At the surface of the magnet natural boundary conditions hold. The potential Ψ_2 satisfies the Laplace equation everywhere and shows a jump at the boundary of the magnetic particle

$$\Psi_2^{int}(r) - \Psi_2^{ext}(r) = \Psi_1(r). \tag{25}$$

These conditions define a double layer potential Ψ_2 which is created by a dipole sheet with magnitude Ψ_1. Ψ_2 can be evaluated using the BE method (Jackson 1982). After discretization, the potential Ψ_2 at the boundary nodes follows from a matrix vector multiplication $\Psi_2 = B\Psi_1$, where B is a $m \times m$ matrix which relates the m boundary nodes with each other. Once Ψ_2 at the boundary has been calculated, the values of Ψ_2 in the particles follow from Laplace's equation with Dirichlet boundary conditions, which again can be solved by a standard FE technique. The matrix B depends only on the geometry and the FE mesh and thus has to be computed only once for a given FE mesh. Since the hybrid FE/BE method does not introduce any approximations, the method is accurate and effective. The use of the BE method easily treats the magnetostatic interactions between distinct magnetic particles and requires no mesh outside the magnetic particles. Suess *et al* (1999) applied the hybrid FE/BE method, in order to simulate the effect of magnetostatic interactions on the reversal dynamics of magnetic nano-elements.

5. Static and dynamic numerical micromagnetic simulations

The use of a magnetic scalar potential in numerical micromagnetic calculations (3), requires one to solve a system of linear equations associated with the magnetostatic boundary value problem (4), whenever the total magnetic Gibb's free energy or the effective field has to be evaluated. An alternative approach to treat the magnetostatic interactions is the use of a magnetic vector potential. Then micromagnetic problems can be reformulated as an algebraic minimization problem with the nodal values of the magnetization angles θ_i, ϕ_i and the nodal values of the magnetic vector potential A as unknowns (2). The simultaneous minimization of the total energy with respect to J and A provides the equilibrium configuration of the magnetization (Aharoni 1996). The integral of (2) is an integration over the entire space and proper techniques to treat the open boundary problem have to be applied. The first variation of (2) gives the unconstrained curl–curl equation for the magnetic vector potential, which is the equation commonly solved in magnetostatic field calculations. Thus, the use of a magnetic vector potential in numerical micromagnetics treats the magnetostatic field in the very same way as conventional FE packages for magnetostatic field calculation (Demerdash 1990).

Either a box scheme or the Galerkin method can be applied to discretize the Gilbert equation of motion (7) in space. This reduces to three ordinary differential equations for each node of the FE mesh, using the box scheme (9) to approximate the effective field. The resulting system of $3N$ ordinary differential equations describes the motion of the magnetic moments at the nodes of the FE mesh. The system of ordinary differential equations is commonly solved using a predictor corrector method or a Runge–Kutta method for mildly stiff differential equations. Small values of the Gilbert damping constant α or a complex microstructure will require a time step smaller than 10 fs, if an explicit scheme is used for the time integration. In this highly stiff regime, backward difference schemes allow much larger times steps and considerably reduce the required CPU time. An implicit time integration scheme can be derived, applying the Galerkin method directly to discretize the Gilbert equation (7). A backward difference method (Hindmarsh 1995) is used for time integration of the resulting system of ordinary differential equations. Since the stiffness arises mainly from the exchange term, the magnetostatic field can be treated explicitly. During a time interval τ, the Gilbert equation is integrated with a fixed magnetostatic field using a higher order backward difference method. The magnetostatic field is updated after time τ, which is taken to be inversely proportional to the maximum torque $\max_i |J_i \times H_{eff,i}|$ over the FE mesh. The hybrid FE/BE method is used to calculate the magnetostatic field. In highly stiff regimes, the semi-implicit scheme requires less CPU time as compared to a Runge–Kutta method, despite the need to solve a system of nonlinear equations at each time step. A semi-implicit time integration scheme was applied to calculate the magnetization reversal dynamics of patterned Co elements, taking into account the small-scale, granular structure of the thin film elements (Schrefl 1999c). Dynamic micromagnetic calculations using the FE method and backward difference were originally introduced by Yang (1996) and applied to study the magnetization reversal dynamics of interacting ellipsoidal particles (Yang 1998).

6. Numerical simulations of NiFe and granular Co elements

Patterned magnetic elements used in random access memories (MRAM) and future sensor applications require a well defined switching characteristic (Kirk 1999). The switching speed of magnetic devices has been of interest since the application of magnetic core memories. Recently, experimental measurements as well as numerical
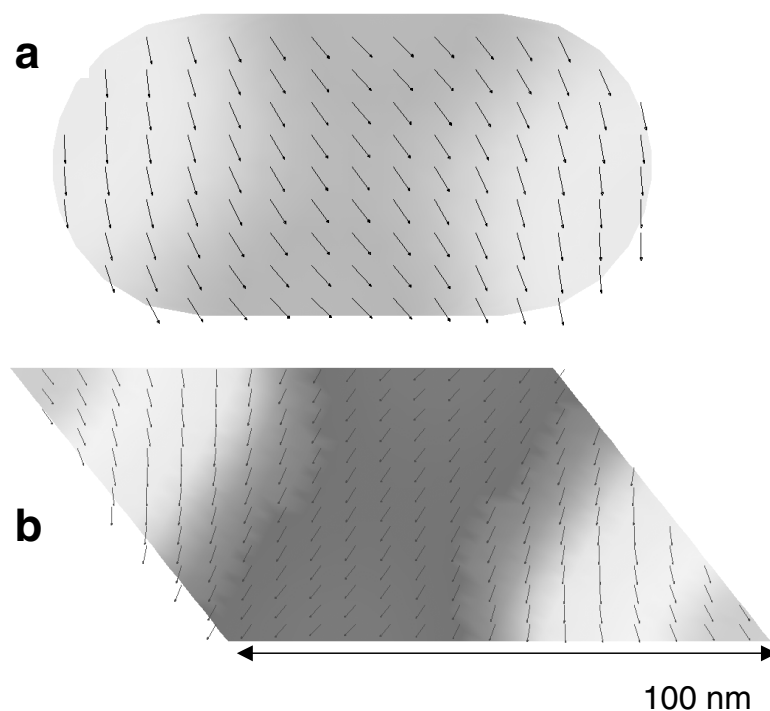
Figure 4. Top view of polarization patterns during the switching of the elements with rounded (a) and slanted ends (b), assuming an extension of $100 \times 50 \times 10$ nm^3 and a Gilbert damping constant of $\alpha = 0, 2$. The external field $H_{ext} = -80$ kA m^{-1} is applied at an angle of $5°$ with respect to the long axis.

micromagnetic simulations (Russek 1999, Gadbois 1998, Koch 1998) were applied to analyse the reversal modes and switching times of MRAM memory cells. Russek (1999) showed that it is possible to successfully switch pseudo-spin valve memory devices with a width of 400–800 nm with pulses whose full width at half maximum is 0.5 ns. Gadbois *et al* (1998) investigated the influence of tapered ends and edge roughness on the switching threshold of memory cells. Koch *et al* (1998) compared experimental results with micromagnetic simulations of the switching speeds of magnetic tunnel junctions. In a theoretical study, Kikuchi (1956) investigated the dependence of the switching time on the Gilbert damping constant α. Solving the Gilbert equation of motion, he derived the critical value of α which minimizes the reversal time. The critical damping occurs for $\alpha = 1$ and $\alpha = 0.01$ for uniform rotation of the magnetization in a sphere and an ultra-thin film, respectively.

Using the hybrid FE/BE method (Schrefl 1997b), we investigated the influence of size and shape on the switching dynamics of sub-micron thin-film NiFe elements. The numerical integration of the Gilbert equation of motion provides the time resolved magnetization patterns during the reversal of elements with flat, rounded, and slanted ends. A Runge–Kutta method, optimized for mildly stiff differential equations (Sommeijer 1998), proved to be effective for the simulation using a regular FE mesh and $\alpha \geqslant 0.2$. However, for an irregular mesh as required for elements with rounded ends and a Gilbert damping constant $\alpha = 0.1$ a time step smaller than 10 fs is required to obtain an accurate solution with the Runge–Kutta method. In this highly stiff regime, backward difference schemes allow much larger time steps and thus the required CPU time remains considerably smaller
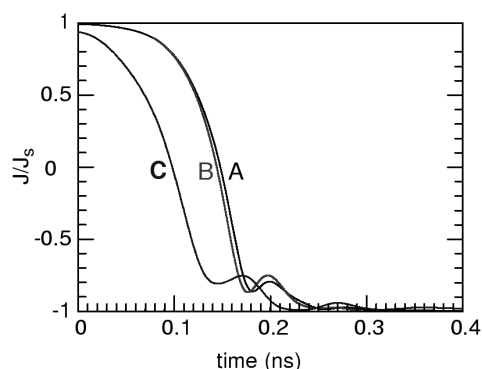

Figure 5. Time evolution of the magnetization component parallel to the field direction for a 2:1 aspect ratio NiFe element with flat (A), rounded (B), and slanted (C) ends with an extension of $100 \times 50 \times 10$ nm^3.

than with the Runge–Kutta method. Since the stiffness arises mainly from the exchange term, the demagnetizing field can be treated explicitly and thus is updated after a time interval τ. During the time interval τ the Gilbert equation is integrated with a fixed demagnetizing field using a higher order backward difference method. τ is taken to be inversely proportional to the maximum torque acting over the FE mesh.

Figure 4 compares the transient state during magnetization reversal of a NiFe thin film element with rounded and slanted shapes. A spontaneous magnetic polarization of $J_s = 1$ T, an exchange constant of $A = 10^{-11}$ J m^{-1} and zero magnetocrystalline anisotropy were assumed for the calculations. The extension of the tetrahedron elements was smaller or equal 5 nm, which corresponds to the exchange length of the material. At first the remanent state of the elements was
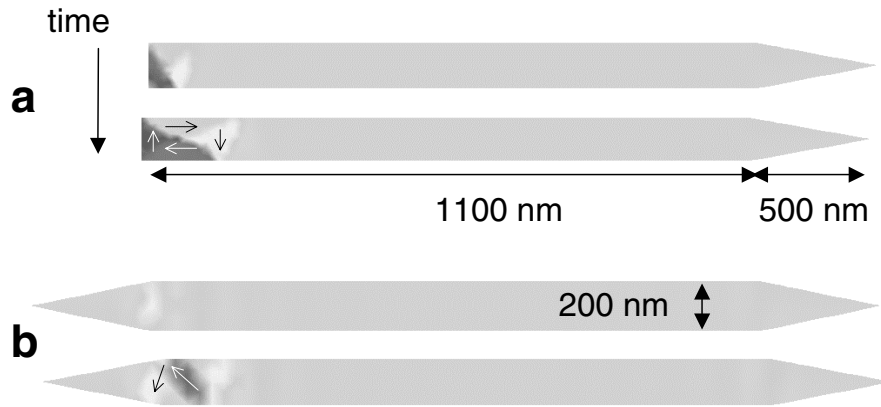
Figure 6. (a) Vortex domain formation at an applied field of 19 kA m^{-1} for an elongated NiFe nano-element with 10 nm thickness. (b) Magnetization reversal in a two-pointed elongated element, in which the end domain formation is suppressed at $H_{ext} = 43$ kA m^{-1}.
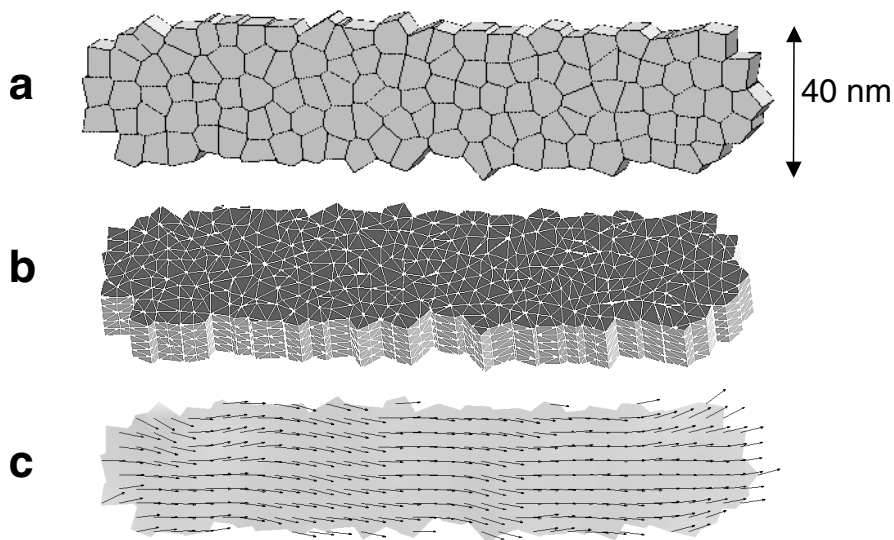

Figure 7. (a) Microstructure of the polycrystalline Co element with $200 \times 40 \times 25$ nm^3. (b) FE discretization of the element. (c) Magnetization ripple structure for zero applied field.

calculated solving the Gilbert equation for zero applied field. The initial state for these calculations was a 'C'-like domain pattern. This procedure is believed to provide the minimum energy state for zero applied field. Then a reversed field of $H_{ext} = 80$ kA m^{-1} was applied at an angle of 5° with respect to the long axis of the particles. Figure 5 gives the time evolution of the magnetization component parallel to the field direction during the switching process for the NiFe elements with an extension of $100 \times 50 \times 10$ nm^3 and a Gilbert damping constant of $\alpha = 0.2$ and clearly shows the effect of the element symmetry on magnetization reversal. Switching occurs by nonuniform rotation of the magnetization. The elements with slanted ends show the fastest switching speed. As compared to the other elements the magnetization remains nearly uniform during the reversal process, which reduces the switching time. After the rotation of the magnetization towards the direction of the applied field, the magnetization precesses around the direction of the effective field. As a consequence the magnetization as a function of time shows oscillations. Micromagnetic FE simulations show that the shape, the size, and the damping constant significantly influence the switching behaviour of thin-film elements.

Submicron NiFe elements with an extension of $200 \times 100 \times 10$ nm^3 switch well below 1 ns for an applied field of 80 kA m^{-1}, assuming a Gilbert damping constant of 0.1. The elements are reversed by nonuniform rotation. Under the influence of an applied field, the magnetization starts to rotate near the ends, followed by the reversal of the centre. This process only requires about 0.1 ns. In what follows, the magnetization component parallel to the field direction shows oscillations which decay within a time of 0.4 ns. The excitation of spin waves originates from the gyromagnetic precession of the magnetization around the local effective field. A much faster decay of the oscillations occurs in elements with slanted ends, where surface charges are caused in the transverse magnetostatic field. The time required for the initial rotation of the magnetization decreases with decreasing damping constant and is independent of the element shape. However, the element shape influences the decay rate of the oscillations. A rapid decay is observed in elements with slanted ends.

Magnetic nano-elements may be the basic structural units of future patterned media or magneto-electronic devices. The switching properties of acicular nano-elements
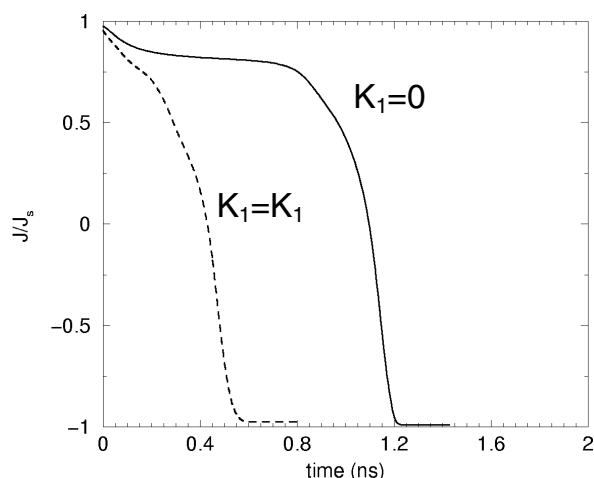
Figure 8. Time evolution of the magnetic polarization parallel to the field direction (long axis) during the reversal of Co elements for zero and random magnetocrystalline anisotropy under the influence of a reversed field of 140 kA m^{-1}, using a Gilbert damping constant $\alpha = 1$.

significantly depend on the aspect ratio and shape of the ends. Pointed ends suppress the formation of end domains in the remanent magnetic state of NiFe nano-elements (Schrefl 1997a). As a consequence the switching field decreases by a factor of 1/2 as compared to elements without blunt ends. Figure 6(a) shows the vortex formation at the blunt ends of an elongated NiFe element as magnetization reversal is initiated. In bars with one pointed end, the formation of the domains starts from the flat ends. Once vortices are formed, they easily break away from the edges causing the reversal of the entire element. Narrow elements with a width smaller than 200 nm remain in a nearly single-domain state. Pointed ends suppress the formation of domains in NiFe elements (figure 6(b)). The simulations predict a spread in the switching field due to magnetostatic interactions of the order of 8 kA m^{-1} for an array of neighbouring 200 nm wide, 3500 nm long and 26 nm thick NiFe elements with a centre-to-centre spacing of 250 nm.
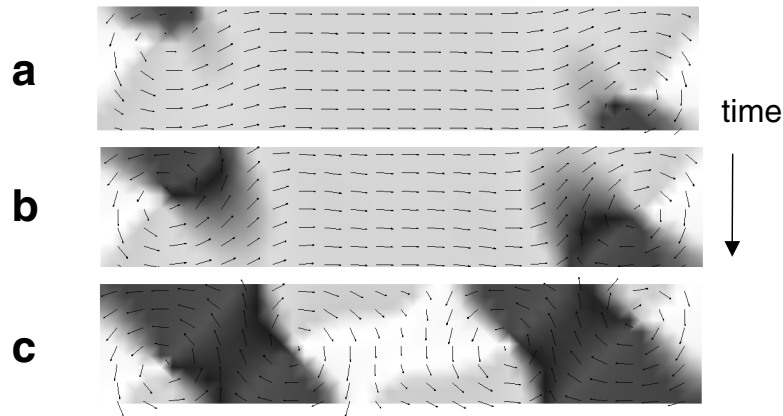
In elements with zero magnetocrystalline anisotropy and in elements with random magnetocrystalline anisotropy, magnetization reversal occurs by the formation and motion of vortices. However, in granular Co elements with random magnetocrystalline anisotropy, vortices form immediately after the application of a reversed field. For zero magnetocrystalline anisotropy a vortex breaks away from the edge only after a waiting time of about 0.8 ns. A similar behaviour was found by Leineweber and Kronmüller (1999) in small hard magnetic particles, where a waiting time after the application of an applied field occurred, before the nucleation of reversed domains is initiated. Figure 7 shows schematically the microstructure of the polycrystalline Co element with a size of $100 \times 40 \times 25$ nm^3. The FE simulation shows that the polycrystalline microstructure significantly influences the magnetization reversal process. Edge irregularities and the random anisotropy reduce both coercive field and switching time as compared to reference calculations, assuming zero magnetocrystalline anisotropy. Figure 8 compares the time evolution of the magnetization

for the Co element with random and zero magnetocrystalline anisotropy. The competitive effects of shape and random crystalline anisotropy lead to a magnetization ripple structure at zero applied field. Sharp edge irregularities help to create vortices, which will move through the width of the element. This process starts at a reversed field $H_{ext} = -95$ kA m^{-1} and leads to the reversal of half of the particle. Following that, a second vortex forms and the entire Co element becomes reversed. Reference calculations using the irregular geometry and zero magnetocrystalline anisotropy reveal a switching field of $H_s = -110$ kA m^{-1} as compared to $H_s = -140$ kA m^{-1} for a regular geometry and zero anisotropy and $H_s = -96$ kA m^{-1} for irregular geometry and random anisotropy. The ease of vortex formation also reduces the switching time. The magnetization reversal was calculated for a constant applied field of $H_{ext} = -140$ kA m^{-1}, using the minimum energy state at zero applied field as the initial state for the dynamic calculations. The analysis of the transient states given in figures 9 and 10 shows that magnetization reversal occurs by the formation and motion of the vortices in both samples. For zero magnetocrystalline anisotropy and an external field close to the coercive field a vortex breaks away from the edge, only after a waiting time of about 0.8 ns. Increasing the external field from $H_{ext} = -140$–190 kA m^{-1} drastically reduces the waiting time. Controlling the time evolution of the micromagnetic energy contributions during magnetization reversal shows that the formation of vortices leads to an increase in the exchange energy during the reversal process.

7. FE simulation of small- and large-grained hard magnets

7.1. High energy density Nd$_2$Fe$_{14}$B permanent magnets

The coercive field of high-performance Nd–Fe–B based magnets is determined by the high uniaxial magnetocrystalline anisotropy as well as the magnetostatic and exchange interactions between neighbouring hard magnetic grains. The long-range dipolar interactions between misaligned grains are more pronounced in large-grained magnets, whereas short-range exchange coupling reduces the coercive field in small-grained magnets (figure 11). FE models of the grain structure are obtained from a nucleation and growth model and subsequent meshing of the polyhedral regions. Numerical micromagnetics at a subgrain level involves two different length scales which may vary by orders of magnitude. The characteristic magnetic length scale on which the magnetization changes its direction is given by the exchange length in soft magnetic materials and the domain wall width in hard magnetic materials. For a wide range of magnetic materials, this characteristic length sale is in the order of 5 nm, which should be significantly smaller than the grain size. The simulation of grain growth using a Voronoi construction (Preparata 1985) yields a realistic microstructure of a hard magnet. Starting from randomly located seed points the grains are assumed to grow with constant velocity in each direction. Then the grains are given by the Voronoi cells surrounding each point. The Voronoi cell of seed point k contains all points of space which are closer to seed point k than to any other seed point.

Figure 9. Transient states during the reversal of a Co element with zero magnetocrystalline anisotropy under the influence of a constant reversed field of 140 kA m^{-1}. Vortexes break away from the flat ends only after a waiting time of about 0.8 ns.
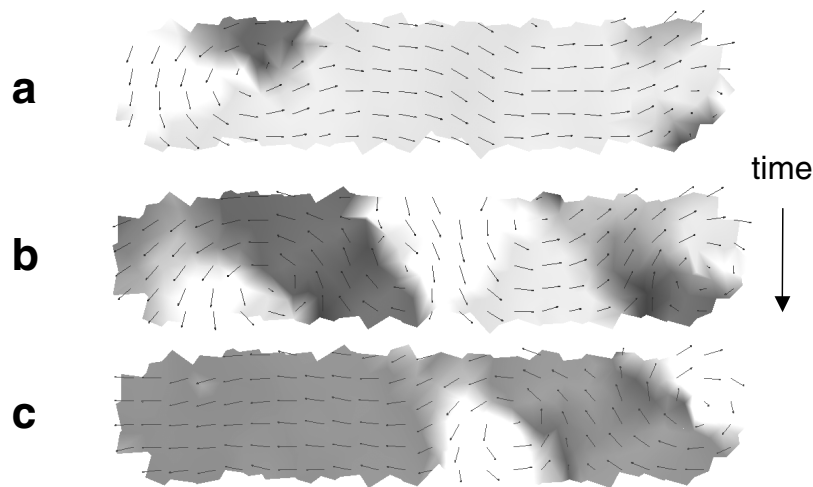
Figure 10. Transient states during the reversal of the granular Co element with random magnetocrystalline anisotropy under the influence of a constant reversed field of 140 kA m^{-1}. at an applied field of 95 kA m^{-1}. The decrease in the switching field has to be attributed to both edge irregularities and random anisotropy.

In order to avoid strongly irregular shaped grains, it is possible to divide the model magnet into cubic cells and to choose one seed point within each cell at random. Different crystallographic orientations and different intrinsic magnetic properties are assigned to each grain. In addition, the grains may be separated by a narrow intergranular phase (Fischer 1998a). Once the polyhedral grain structure is obtained, the grains are further subdivided into finite elements. An example is the 2D grain structure of figure 12 with an overlay of the triangular mesh inside the grains and outside the magnet (Schrefl 1992). The polarization is defined at the nodal points of the FE mesh. Within each element the polarization is interpolated by a polynomial function. Thus, the magnetic polarization $J(r)$ may be evaluated everywhere within the model magnet, using the piecewise polynomial interpolation of the polarization on the FE mesh.

High energy density Nd–Fe–B magnets ($BH_{max} > 400$ kJ m^{-3}) are produced by the sintering technique, which leads to grain sizes above 1 μm (Sagawa 1984). The doping of elements changes the phase relation and favours the formation of new phases. Additional secondary nonmagnetic intergranular phases decrease the remanence and interrupt the magnetic interactions between the grains, thereby improving
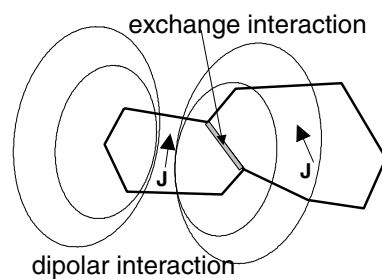

Figure 11. Long-range dipolar interactions and short-range exchange coupling between misaligned magnetic grains.

the coercivity of large-grained sintered magnets (Fidler 1997). In magnets with higher Nd concentrations, grain size, misorientation and distribution of grains control the coercive field. The higher the Nd content of the magnet and therefore the volume fraction of the Nd-rich intergranular phase, the more reduced is the contribution of the exchange and also dipolar coupling between the grains. In contrast to the Stoner–Wohlfarth theory (Stoner 1948), the coercive field will increase with decreasing alignment of the easy
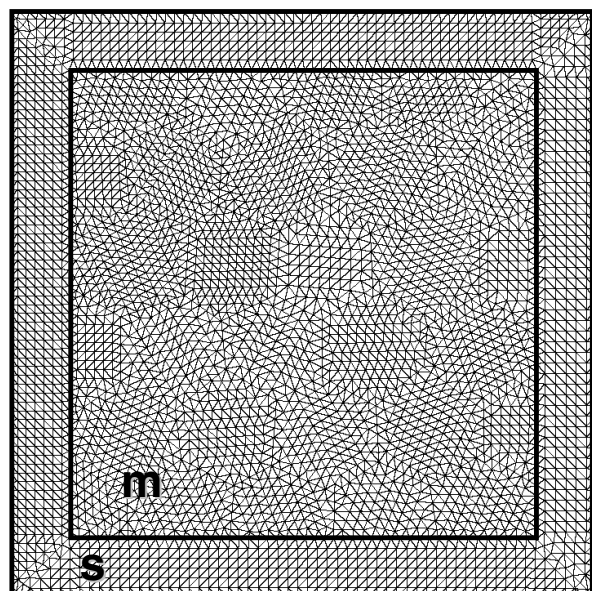
Figure 12. 2D model of the granular microstructure obtained by a Voronoi construction. The triangular FE mesh is overlaid inside the grains (m) and outside the magnet (s).

axis if the anisotropy is reduced near the grain boundaries. The FE simulations confirm the experimental results that nonmagnetic Nd-rich phases at grain boundary junctions significantly increase the coercive field. Micromagnetic 3D FE calculations were used to simulate the influence of Nd-rich phases located at grain boundary junctions, reduced anisotropy near the grain boundaries, and the degree of misalignment on the nucleation of reversed domains. Figure 13(a) shows the 3D model of the FE model and the generated mesh near the junction of neighbouring grains. For a perfect microstructure the numerical results agree well with the Stoner–Wohlfarth theory. The most misoriented grain, which has the largest angle between the c-axes and the alignment direction, determines the coercive field. The coercive field decreases with increasing misalignment. A reduction in the magnetocrystalline anisotropy near the grain boundaries leads to a linear decrease in the coercive field. The coercive field decreases from 3200 to 900 kA m^{-1} as the anisotropy constant in a 6 nm thick region near the grain boundaries is reduced from its bulk value to zero. The reduction in the magnetocrystalline anisotropy reverses the dependence of the coercive field on the degree of alignment. The coercive field increases by about 80 kA m^{-1} as the misalignment angle is changed from 8° to 16°. This effect has to be attributed to a higher demagnetizing field in the well aligned sample, which initiates the nucleation of reversed domains into the defect region. The FE analyses confirm that nonmagnetic Nd-rich phases at grain boundary junctions significantly increase the coercive field. The coercive field increases by about 15% as a nonmagnetic Nd-rich phase near the grain boundary junctions is taken into account. The simulations show that the presence of the Nd-rich phase significantly changes the exchange and the magnetostatic interactions. As a consequence, the nucleation of reversed domains is suppressed. The simulations allow the identification of the regions within the microstructure
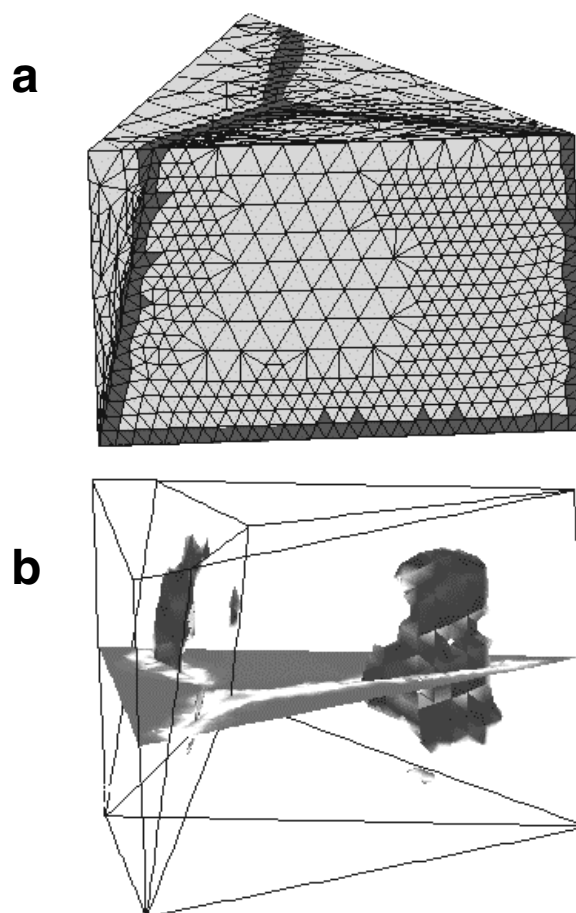

Figure 13. (a) 3D FE model of the grain boundary junction of neighbouring hard magnetic grains. For the calculations, the misalignment of the grains was varied from 8° to 16°. The isosurfaces (b) show the regions, where reversed domains are nucleated at $H_{ext} = -960$ kA m^{-1} assuming $K_1 = 0$ in the intergranular region.
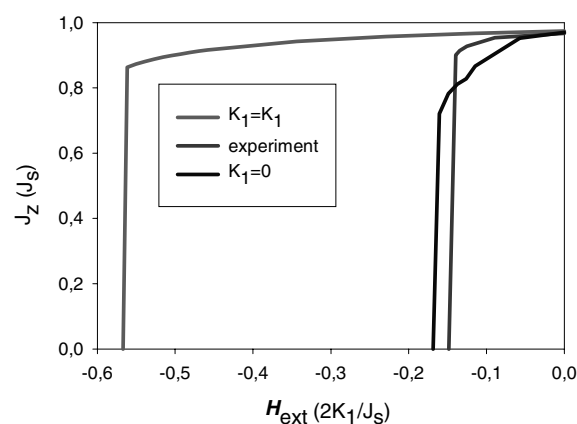
Figure 14. Comparison of simulated and experimental demagnetization curves of high remanent $Nd_2Fe_{14}B$ magnets. The calculated curves assume bulk values and zero magnetocrystalline anisotropy of the intergranular region between the hard magnetic grains.

where reversed domains are nucleated (figure 13(b)). The comparison with experimental data provides a detailed understanding of magnetization reversal in high energy
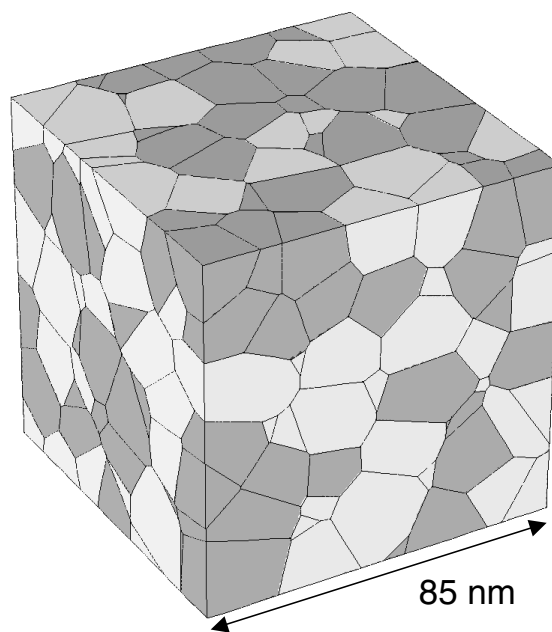
Figure 15. Grain structure model of 343 grains of a multi-phase nanocrystalline $Nd_2Fe_{14}B/(Fe_3B, \alpha\text{-Fe})$ magnet resulting from a Voronoi construction used for the FE simulations.

density permanent magnets. The demagnetization curves of figure 14 compare perfect grain boundaries, distorted grain boundaries and experimental data. The influence of the magnetocrystalline anisotropy of the intergranular region on the coercive field is clearly shown. The simulations explain experimental data, which show a decrease in the coercive field with increasing misalignment (Kim 1994). Similar numerical results were obtained by Bachmann *et al* (1998), who used a FE method combined with an atomic exchange interaction model based on the Heisenberg model for localized interacting magnetic moments in a system with small grain size (< 100 nm).

7.2. Nanocrystalline, composite $Nd_2Fe_{14}B/(\alpha\text{-Fe}, Fe_3B)$ magnets

Exchange interactions between neighbouring soft and hard grains lead to remanence enhancement of isotropically oriented grains in nanocrystalline composite magnets (Davies 1996, McCallum 1987, Coehoorn 1989, Hadjipanayis 1988, McCormick 1998, Kanekiyo 1993, Kuma 1998). Nanocrystalline, single-phase Nd–Fe–B magnets with isotropic alignment show an enhancement of remanence by more than 40% as compared to the remanence of noninteracting particles, if the grain size is of the order of 10–30 nm. Our numerical micromagnetic calculations have revealed that the interplay of magnetostatic and exchange interactions between neighbouring grains influence the coercive field and remanence considerably (Schrefl 1994a, b, 1997c, 1998, 1999b). Soft magnetic grains in two- or multi-phase, composite permanent magnets cause a high polarization, and hard magnetic grains induce a large coercive field, provided that the particles are small and strongly exchange coupled. Figure 15 shows a typical grain structure model of 343 grains resulting from grain

growth simulation using a Voronoi construction used for the FE simulations. This model was used to calculate the influence of the volume fraction of the different phases ($Nd_2Fe_{14}B$, Fe_3B, and $\alpha\text{-Fe}$) and the grain size on the hysteresis properties. Theoretical limits for remanence and coercivity were derived by numerical micromagnetic Fe simulations for $Nd_2Fe_{14}B/(Fe_3B, \alpha\text{-Fe})$ nanocrystalline permanent magnets. The coercive field shows a maximum at an average grain size of 15–20 nm. Intergrain exchange interactions override the magnetocrystalline anisotropy of the $Nd_2Fe_{14}B$ grains for smaller grains, whereas exchange hardening of the soft phases becomes less effective for larger grains. The magnetization distribution at zero applied field for different grain sizes, clearly shows that remanence enhancement increases with decreasing grain size. Owing to the competitive effects of magnetocrystalline anisotropy and intergrain exchange interactions, the magnetization of the hard magnetic grains significantly deviates from the local easy axis for a grain size $D \leqslant 20$ nm. Regions with a deviation angle greater than $40°$ may cover entire hard magnetic grains for $D = 10$ nm. As a consequence coercivity drops, since intergrain exchange interactions help to overcome the energy barrier for magnetization reversal. With increasing grain size the magnetization becomes nonuniform, following either the magnetocrystalline anisotropy direction within the hard magnetic grains or forming a flux closure structure in soft magnetic regions. Neighbouring $\alpha\text{-Fe}$ and Fe_3B grains may make up large continuous areas of soft magnetic phase, where magnetostatic effects will determine the preferred direction of the magnetization. The large soft magnetic regions deteriorate the squareness of the demagnetization curve and cause a decrease in the coercive field for $D > 20$ nm. A vortex-like magnetic state with vanishing net magnetization will form within the soft magnetic phase, if the diameter of the soft magnetic region exceeds 80 nm. Figure 16 presents the calculated magnetization distribution in a slice plane of a 40 vol% $Nd_2Fe_{14}B$, 30 vol% $\alpha\text{-Fe}$, and 30 vol% Fe_3B magnet with a mean grain size of 30 nm for zero applied field. The magnetic polarization J remains parallel to the saturation direction within the soft magnetic grains, whereas it rotates towards the direction of the local anisotropy direction within the hard magnetic grains. The demagnetization curves of figure 17 give the contributions of the different phases ($\alpha\text{-Fe}$, Fe_3B, $Nd_2Fe_{14}B$), in addition to the total magnetic polarization. The numerical integration of the Gilbert equation yields the transient magnetic states during irreversible switching and thus reveal how reversed domains nucleate and expand. The comparison of the demagnetization curves and the magnetization distribution clearly shows that irreversible processes are associated with the irreversible switching of hard magnetic grains. Magnetization reversal is dominated by the rotation of the magnetic moments within the soft magnetic grains. During this process, the magnetic polarization of the soft phase remains correlated within an area covering several $\alpha\text{-Fe}/Fe_3B$ grains. This collective behaviour of neighbouring soft magnetic grains has to be attributed to exchange interactions. The magnetocrystalline anisotropy hinders the rotation of J within the hard phase, leading to a high exchange energy density at the interface
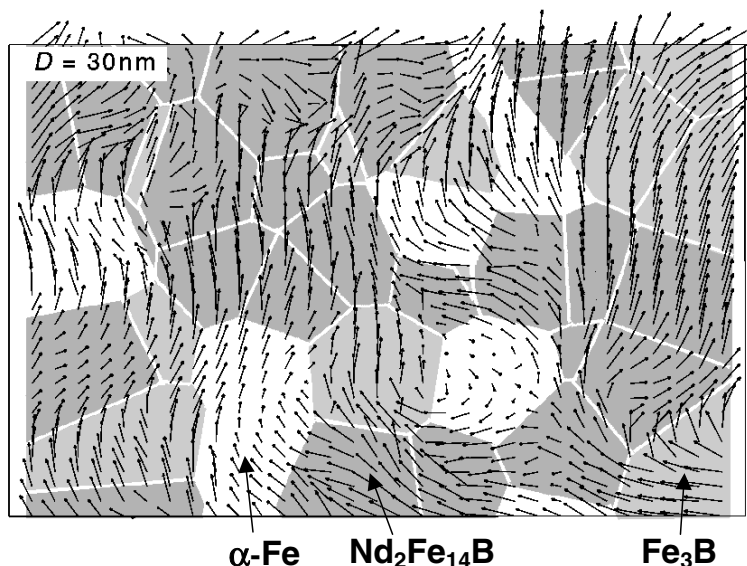
Figure 16. Magnetization distribution in a slice plane of a 40 vol% $Nd_2Fe_{14}B$, 30 vol% α-Fe, and 30 vol% Fe_3B magnet with a mean grain size of 30 nm for zero applied field. The arrows denote the magnetization direction projected on a slice plane and show a vortex-like state after irreversible switching.
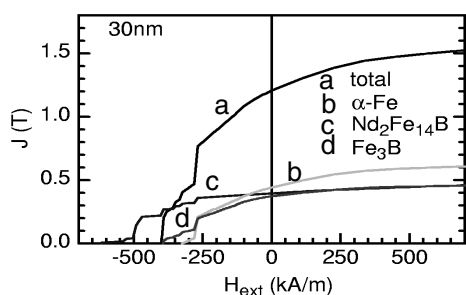
Figure 17. Numerically calculated demagnetization curves of the various contributions of a 40 vol% $Nd_2Fe_{14}B$, 30 vol% α-Fe, and 30 vol% Fe_3B magnet with a mean grain size of 30 nm.

between the different phases. When the expense of exchange energy becomes too high, a reversed domain nucleates within the $Nd_2Fe_{14}B$ grain and the entire hard magnetic grain becomes reversed.

The calculations show a linear trade off of remanence and coercivity as a function of the α-Fe to Fe_3B ratio. The coercive field H_c and the remanence J_r cover the range of $(H_c, J_r) = (340 \text{ kA m}^{-1}, 1.4 \text{ T})$ to $(610 \text{ kA m}^{-1}, 1.1 \text{ T})$ for a composite magnet containing 40% $Nd_2Fe_{14}B$, $(60-x)$% Fe_3B and x% α-Fe. The replacement of α-Fe with Fe_3B improves the coercive field without a significant loss in the remanence. The substitution of Nd by Tb or Dy increases the hard phase anisotropy and reduces the saturation polarization. The coercivity of two-phase $Nd_2Fe_{14}B/\alpha$-Fe magnets can be improved by about 30% without a significant loss in remanence. Only a moderate change in the intrinsic magnetic properties of the hard phase is required, in order to achieve this increase in the coercive field. A large number of papers have been published so far and several authors have predicted remanence enhancement and the reduction of the coercive field in nanocrystalline permanent magnets, using analytical micromagnetic calculations or 2D or 3D FD or FE methods

(Kneller 1991, Skomski 1993, Fischer 1998b, Fukunaga 1992, Leineweber 1997).

7.3. Precipitation hardened, high-temperature $Sm(Co, Cu, Fe, Zr)_{7-8}$ magnets

The search for novel soft and hard magnetic materials for high-temperature advanced power applications is an active area of research worldwide. The increase in the operating temperature of motors, generators and other electronic devices leads to an improvement in their efficiency. In the development of high-temperature magnets the activities concentrate on the improvement of precipitation hardened $Sm(Co, Fe, Cu, Zr)_{7-8}$ magnets and the search for new compounds with sufficiently high values of magnetization and coercive field at elevated temperatures. A new series of magnets with H_c up to 1050 kA m^{-1} at 400 °C has been developed (Liu 1999, Tang 2000). These magnets have low-temperature coefficients of H_c and a straight line B versus H (extrinsic) demagnetization curve up to 550 °C. High Cu, low Fe and a higher Sm concentration were found to contribute to high coercivity at high temperatures. TEM investigations show a cellular precipitation structure of about 60×120 nm in size (Fidler 1983, Streibl 2000). The rhombic cells of the type $Sm(Co, Fe)_{17}$ are separated by a $Sm(Co, Cu, Zr)_{5-7}$ cell boundary phase. The development of the continuous, cellular precipitation structure is controlled by the growth process and the chemical redistribution process and is determined by the direction of zero deformation strains due to the lattice misfit between the different phases.

A 3D FE method was used to simulate domain wall pinning in $SmCo_5/Sm_2Co_{17}$ based permanent magnets. The FE model (figure 18(a)) was built according to the cellular microstructure obtained from TEM investigations. During magnetization reversal the domain walls become pinned at the continuous cell boundary phase. Depinning of the domain wall starts at the corners of the cell structure
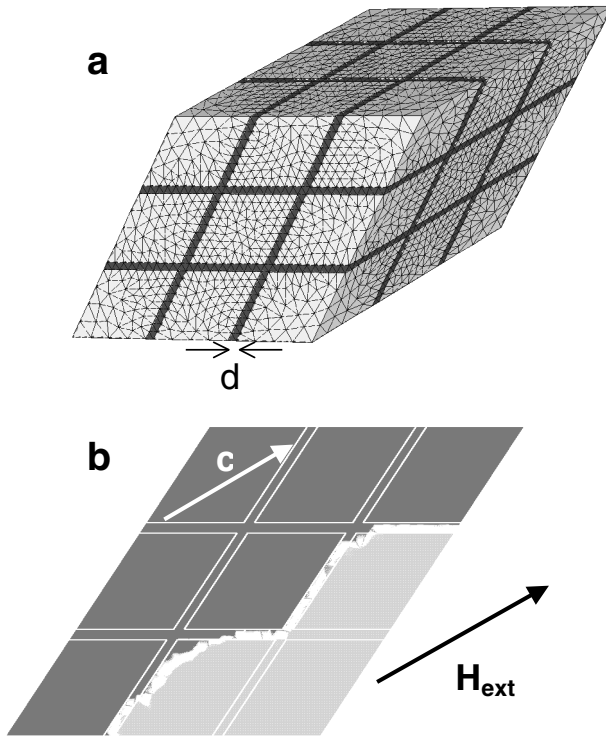
Figure 18. (a) FE model used for the 3D micromagnetic simulation of a high-temperature magnet consisting of a continuous Sm(Co, Cu)$_{5-7}$ precipitation structure with width d and 27 Sm$_2$(Co, Fe)$_{17}$ rhombic cells (b). Calculated domain image showing the depinning of a domain wall at $H_{ext} = 2300$ kA m^{-1} for a cell size of 160 nm.
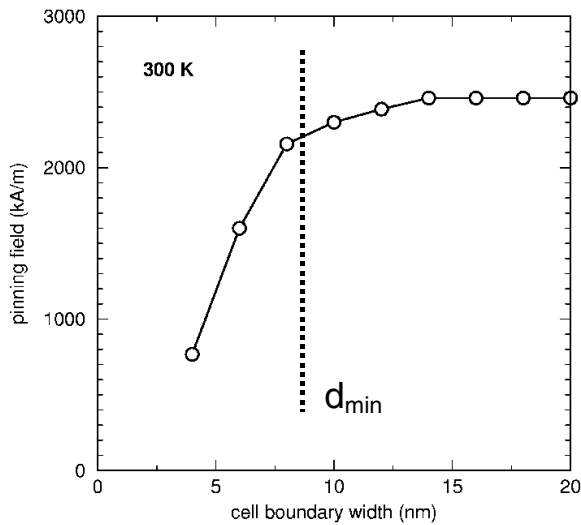
Figure 19. Calculated pinning field as a function of the cell boundary width of a precipitation hardened, high-temperature Sm(Co, Cu, Fe, Zr)$_{7-8}$ magnet. A minimum thickness d_{min} of the precipitation structure is necessary in order to obtain a high pinning field.

(figure 18(b)). The numerical results show a strong influence of the dimension of the cell boundary phase on the coercive field, which significantly increases with the extension of the 1:5/7-type cell boundary phase. The calculated values of the coercive field are in the range from 1000 to 2000 kA m^{-1}, assuming a cell size varying from 80 to

160 nm. The difference in the magnetocrystalline anisotropy between cell boundary and cell interior phases is determined by the composition (especially the Cu content) of the magnet. Three-dimensional micromagnetic simulation reveals that the pinning field strongly depends on the intrinsic properties (J_s, K, A). A minimum width of the cell boundary phase is necessary to obtain high pinning fields (figure 19). Exact precipitation structure parameters (controlled by composition and processing) and the exact values of $J_s(T)$, $K_1(T)$ and $A(T)$ are necessary to explain the coercive field at high temperature.

8. Future trends

8.1. FE-adaptive mesh refinement

The FE method effectively treats magnetization processes in samples with arbitrary geometries or irregular microstructures. Adaptive refinement schemes allow the magnetization distribution to be resolved on a subgrain level, improving the accuracy of the solution while keeping the computational effort to a minimum. Recently, FE mesh refinement was applied in micromagnetic simulations of longitudinal thin film media (Tako 1997), domain structures in soft magnetic thin films (Hertel 1998), and domain wall motion in permanent magnets (Scholz 1999). The discretization of the micromagnetic equations gives rise to two types of discretization errors. One is associated with the evaluation of the exchange field, the other arises from the FE computation of the magnetostatic field. Improvements in the micromagnetic resolution can be made by a uniform increase in the level of discretization. However, this places more computational nodes in areas where the magnetization remains uniform. Ideally, it would be most efficient to place new nodes where the error is highest. The aim of adaptive mesh refinement schemes is to obtain a uniform distribution of the discretization error over the FE mesh (Penman 1987). In order to decide where to refine the mesh, refinement indicators should give a good estimate of the local error. A second criterion for the selection of error estimators for adaptive meshing are the computational costs. Error estimators should be cheap to evaluate and thus error indicators derived from the current FE solution on an element-by-element basis are preferred.

Within the framework of micromagnetism (Brown 1963a, Aharoni 1996), the magnitude of $\boldsymbol{J}$ is assumed to be a constant over the whole magnet, which depends only on the temperature

$$|\boldsymbol{J}| = J_s(T). \tag{26}$$

This condition can only hold at the nodal points of the FE mesh. The linear interpolation (equation (15)) does not preserve the magnitude of the magnetization within a finite element. Bagneres-Viallix et al (1991) proposed to use the deviations of the length of the magnetization vector from the centre of an element as the refinement indicator. The magnetization distribution of a one-dimensional domain wall can be calculated analytically. Thus, the true discretization error of the FE solution can be evaluated. Numerical investigations of one-dimensional mesh refinement showed that the error estimator based on the norm of the magnetization shows the very same functional

dependence on the number of finite elements as the true error of the solution. However, the deviation of $|\boldsymbol{J}|$ from J_s within an element may be used as an error indicator for adaptive refinement schemes. Successive refinement of elements where $|\boldsymbol{J}|$ deviates from J_s will lead to a fine mesh in areas with large spatial variation of the magnetization direction. After several refinement steps the constraint (equation (26)) will be approximately fulfilled on the entire FE mesh.

Refinement indicators that point out the exchange discretization error are usually based on the spatial variation of the magnetization (Hertel 1998). They identify domain walls, vortices, or magnetic inhomogeneities near edges and corners. In order to consider the discretization error associated with the magnetostatic field calculation, Tako *et al* (1997) suggested a refinement indicator based on the divergence and curl of both the magnetization and magnetic field. Simulating the magnetization structure of two-dimensional magnetic nano-elements, Ridley *et al* (1999) showed that this refinement indicator correctly identifies the regions where the true error in the computed magnetic field is high. In longitudinal thin-film media the granular microstructure significantly influences the remanent magnetization distribution. The adaptive refinement clearly improves both the efficiency and accuracy of the computations of magnetization patterns in thin-film microstructures obtained from a Voronoi construction (Tako 1997). A refinement indicator based on the spatial variation of both magnetization and magnetic field is used to point out elements in which refinement is necessary. Elements which show a refinement indicator greater than 20% of the maximum value over all elements are subdivided by regular division. The numerical results indicate a significant improvement in the calculated magnetization structure after refinement. The magnetization tends to form vortices which do not fully develop in the coarse grid. With further refinement the structure is allowed to attain a lower energy state, allowing a more complete development of the solenoidal structure. During the refinement process the total energy decreases by about 50%, which clearly indicates the success of the refinement indicator. Hertel *et al* (1998) proposed a refinement scheme to resolve vortices in micromagnetic simulations of domain structures in soft magnetic thin-film elements. The discretization error is reduced by moving nodes of the FE mesh towards regions where higher accuracy is needed. In micromagnetic simulations of domain structures in soft magnetic thin films, this was accomplished by shrinking the elements in regions with strong inhomogeneities. Thus, a high mesh density, which results in a high micromagnetic resolution, was obtained near vortices and domain walls, while keeping the number of elements constant.

In hard magnetic materials the magnetization is uniform within magnetic domains, whereas it is highly non-uniform in domain walls, near nucleation sites, vortices or grain boundaries. A coarse mesh may be sufficient in regions, where the magnetization is almost uniform. Local mesh refinement near grain boundaries, domain walls, vortices and nucleation sites significantly reduces the number of degrees of freedom. As domain walls can move due to external fields, the discretization has to be adjusted adaptively during the

simulation. Scholz *et al* (1999) presented an algorithm that adapts the FE mesh to the solution of the Gilbert equation. Refinement of the tetrahedral mesh at the current wall position and coarsening within the bulk of the domains leads to a high-density mesh that moves together with the wall. After each time step, error indicators based on the deviations of $|\boldsymbol{J}|$ from J_s, are calculated for each element. If the maximum error indicator over all elements, η_{max}, exceeds a certain threshold the following refinement scheme is applied: elements, whose error indicators exceeds $0.1\eta_{max}$ are marked for refinement, whereas elements with an error indicator lower than $0.01\eta_{max}$ are marked for coarsening. Then, the FE mesh is refined by subdividing elements, which are marked for refinement. Coarsening is effected by removing finite elements which have been created by an earlier refinement step (Bey 1995). Figure 20 shows the regions of fine mesh at the current wall position during the simulation of domain wall motion in thin $Nd_2Fe_{14}B$ specimens. The wall moves towards the boundary of a misoriented grain, where it remains pinned owing to a reduction exchange and anisotropy energy stored in the wall.

The presented method provides a reliable technique to simulate domain wall movement with a minimum number of finite elements. The alternate refinement and coarsening reduces the space discretization error and thus avoids domain wall pinning on a too coarse grid. Figure 20 shows an example of FE mesh refinement during the simulation of domain wall motion in a thin polycrystalline $Nd_2Fe_{14}B$ sample. The domain wall becomes pinned at the grain boundary of misoriented grains.

8.2. Thermally activated magnetization reversal processes

New experimental techniques allow spatially resolved measurements of magnetic structures and an investigation of isolated magnetic particles (Wernsdorfer 1997). All this leads to an increasing interest in the understanding of the behaviour of small magnetic particles down to nanometre regime, especially their dynamics during magnetization reversal and their thermal stability. Sufficiently large particles consist of many magnetic domains due to demagnetization effects. With decreasing size the single-domain state becomes energetically favourable for particles with typical sizes much less than 1 μm. Smaller particles in the range of only a few nanometres become superparamagnetic, which means that they are thermally unstable (Brown 1963b, Coffey 1998, Nowak 1999), since the energy barriers blocking the magnetization reversal are small enough here to be overcome by thermal fluctuations at room temperature. This effect is thought to limit the density of information storage. Hence, the understanding of the role of thermal activation for the dynamical behaviour of ferromagnetic particles is one of the most important subjects of modern micromagnetism. It is interesting from a fundamental point of view as well as for practical applications in information storage devices. For still smaller particles, which then consist only of a rather small number of atoms, quantum effects set in, leading to magnetization reversal by tunnel effects. Variational methods are used in continuum micromagnetic
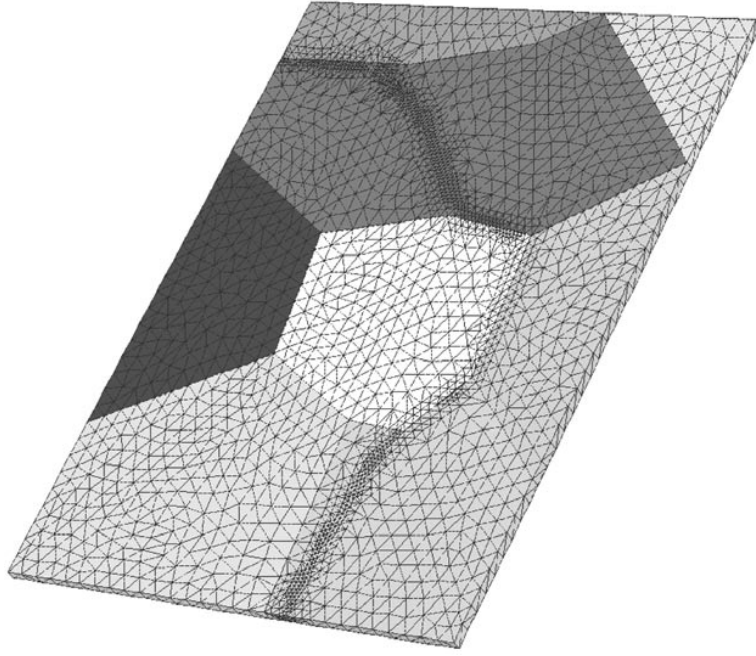
Figure 20. Granular microstructure and adaptive mesh refinement in the region of a moving domain wall, which becomes pinned at the grain boundaries of misoriented grains.

theories to determine the minimum Gibbs's free energy of the system. Magnetization reversal processes occur when a local energy minimum becomes unstable. The actual path of the magnetization follows from the numerical integration of the Gilbert equation of motion, which resolves the magnetization processes in time and space. Taking into account finite temperature, it is obvious that the magnetization reversal takes place by thermal activation over finite energy barriers. The finite temperature will also influence the high-frequency magnetization reversal. The complex response of the magnetization to rapidly changing applied fields has historically been a problem for high-speed magnetic devices. Projected data storage systems with a frequency greater than 250 MHz will be forced to confirm this challenge directly for both heads and media. Effects of thermal activation are included in micromagnetic simulations by adding a random thermal field to the effective magnetic field H_{eff} (6). As a result, the Landau–Lifshitz equation is converted into a stochastic differential equation of Langevin type with multiplicative noise. The Stratonovich interpretation of the stochastic Landau–Lifshitz equation leads to the correct thermal equilibrium properties. Micromagnetic simulations reveal the details of the magnetization distribution and dynamic magnetization reversal processes. The knowledge of the dynamic behaviour is of great importance for the design of future magnetic recording media. When the desired magnetization switching frequencies reach an order of magnitude which is comparable to the intrinsic relaxation time of the media, the switching dynamics have to be investigated in more detail.

Thermal activation is introduced in the Landau–Lifshitz equation (5) by a stochastic thermal field H_{th}, which is added to the effective field. It accounts for the effects of the interaction of the magnetization with the microscopic degrees of freedom (e.g. phonons, conducting electrons, nuclear

spins, etc), which cause fluctuations of the magnetization distribution. This interaction is also responsible for the damping, since fluctuations and dissipation are related manifestations of one and the same interaction of the magnetization with its environment. Since a large number of microscopic degrees of freedom contribute to this mechanism, the thermal field is assumed to be a Gaussian random process with the following statistical properties:

$$\langle H_{th,i}(t) \rangle = 0 \tag{27}$$

$$\langle H_{th,i}(x,t) H_{th,j}(x',t') \rangle = 2D\delta_{ij}\delta(x-x')\delta(t-t') \tag{28}$$

$$D = \frac{\alpha k_B T}{\gamma J_s}. \tag{29}$$

After adding the thermal field we get the stochastic Landau–Lifshitz equation

$$\frac{\partial J}{\partial t} = -\frac{|\gamma|}{1+\alpha^2}\{J \times (H_{eff} + H_{th})\}$$
$$-\frac{\alpha}{J_s \cdot (1+\alpha^2)}\{J \times [J \times (H_{eff} + H_{th})]\}. \tag{30}$$

Hence, after FE discretization we obtain a system of Langevin equations with multiplicative noise

$$\frac{\partial J_i}{\partial t_i} = A_i(J,t) + \sum_k B_{ik}(J,t) \cdot H_{th,k}(t) \qquad i = 1, \ldots, 3N. \tag{31}$$

The multiplicative factor $B_{ik}(J;t)$ for the stochastic process $H_{th;k}(t)$ is a function of J.

The mechanism of thermally activated magnetization switching in small spherical particles with $J_s = 0.5$ T, $A = 3.64 \times 10^{-12}$ J m^{-1}, $K_1 = 2 \times 10^5$ J m^{-3}, $\alpha = 1$ and a radius of 11.5 nm has been investigated by the FE method (Scholz 2000). The initial magnetization is homogeneous and parallel to the easy axis of the particle. Its magnetization
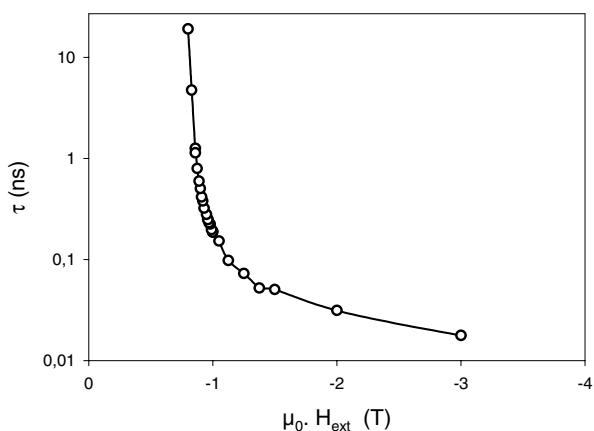
Figure 21. FE simulation of the dependence of the metastable lifetime on the external field for a small spherical particle with $J_s = 0.5$ T, $A = 3.64 \times 10^{-12}$ J m^{-1}, $K_1 = 2 \times 10^5$ J m^{-3}, $\alpha = 1$ and a radius of 11.5 nm.

distribution is destabilized by an external magnetic field, which is parallel to the easy axis (z direction) but antiparallel to the initial polarization. Since this is a metastable state, we can expect the particle to overcome the energy barrier, which is called the activation energy, and reverse its magnetization after some time. The metastable lifetime (or relaxation time) τ is defined as the time, which passes from the initially saturated state $J_z(0) = J_s$ until $J_z(\tau) = 0$. In order to measure the metastable lifetime a large number of simulations have been performed for each set of parameters. After 200 measurements a waiting time histogram was obtained. The integral of this histogram is proportional to the switching probability $P(t)$, which is the probability that the particle has switched by a certain time. However, it is more common to draw graphs for the (rescaled) probability of not switching $P_{not}(t) = 1 - P(t)$. The magnetization reversal process can happen in different reversal modes. In a particle with low anisotropy the polarization rotates coherently, which means that the magnetization remains almost homogeneous during the reversal process except for small thermal fluctuations. If the anisotropy is increased, it becomes favourable to form a nucleus with reversed magnetization. Thus, a droplet nucleates near the surface and expands until the magnetization is completely reversed.

Figure 21 shows how the metastable lifetime decreases when the external field is increased. The reversal mode changes from nonuniform rotation to droplet nucleation as the external field is increased from 0.8 ($2K_1/J_s$) to 1.1 ($2K_1/J_s$). A similar behaviour has been observed in Monte Carlo simulations (Rikvold 1994), where this behaviour is interpreted in terms of droplet theory. The Langevin dynamics approach proved to be a suitable method to model the effects of thermal activation in magnetic materials.

9. Conclusions

Micromagnetism treats magnetic materials as classical continuous media described by appropriate differential equations governing their static and dynamic behaviour. The micromagnetic problem is reasonably well understood in the framework of Brown's equations. The numerical solution

of the governing equations can be effectively performed using FE and related methods which easily handle complex microstructures. FE techniques for an effective solution of the basic static and dynamic equations were compared. These include various methods to treat the so-called open boundary problem in magnetostatic field calculation and discretization schemes that allow sparse matrix methods for the time integration of the equation of motion. FE simulations successfully predict the influence of microstructural features like grain size, particle shape, intergranular phases and surface irregularities on the magnetic properties. Adaptive refinement and coarsening of the mesh controls the discretization error and provides optimal grids for micromagnetic FE simulation of magnetization processes in recording media, vortex formation in soft magnetic thin films and of nucleation and expansion of reversed domains in hard magnetic bulk materials. Theoretical limits for remanence, coercive field, switching behaviour and other properties have successfully been calculated for a large number of materials. Incorporating thermally activated magnetization reversal will predict the upper limits of the switching frequency in thin-film recording media. In the future new computational approaches, including the development of hybrid micromagnetic models such as the Monte Carlo methods, will obtain quantitative treatment of the correlation between the microstructure and the magnetic hysteresis properties of modern magnetic materials in large systems and large timescale regions.

References

Aharoni A 1962 Theoretical search for domain nucleation *Rev. Mod. Phys.* **34** 227–38
——1991 Magnetostatic energy calculation *IEEE Trans. Magn.* **27** 3539–47
——1996 *Introduction to the Theory of Ferromagnetism* (Oxford: Oxford University Press)
Alben R, Becker J J and Chi M C 1978 Random anisotropy in amorphous ferromagnets *J. Appl. Phys.* **49** 1653–8
Asselin P and Thiele A A 1986 On the field lagrangians in micromagnetics *IEEE Trans. Magn.* **22** 1876–80
Bachmann M, Fischer R and Kronmueller H 1998 *Proc. 10th Symp. on Magnetic Anisotropy and Coercivity in Rare Earth Transition Metal Alloys (Dresden)* pp 217–36
Bagneres-Viallix A, Baras P and Albertini J B 1991 2D and 3D calculations of micromagnetic wall structures using finite elements *IEEE Trans. Magn.* **27** 3819–2821
Berkov D V and Gorn N L Quasistatic remagnetization processes in two-dimensional systems with random on-site anisotropy and dipolar interaction—numerical simulations *Phys. Rev.* B **57** 14 332–43
Bey J 1995 Tetrahedral grid refinement *Computing* **55** 355–78
Blank R 1991 What determines the demagnetization in Nd–Fe–B magnets? *J. Magn. Magn. Mater.* **101** 317–22
Boerner E D and Bertram H N 1997 Dynamics of thermally activated reversal in nonuniformly magnetized single particles *IEEE Trans. Magn.* **33** 3052–4

Brown W F Jr 1963a *Micromagnetics* (New York: Wiley Interscience)
——1963b Thermal fluctuations of a single-domain particle *Phys. Rev.* **130** 1677–86
Brunotte X, Meunier G and Imhoff J F 1992 Finite element modelling of unbounded problems using transformations: rigorous, powerful and easy solutions *IEEE Trans. Magn.* **28** 1663–6
Chantrell R W, Hannay J D, Wongsam M, Schrefl T and Richter H-J 1998 Computational approaches to thermally activated fast relaxation *IEEE Trans. Magn.* **34** 1839–44
Chen Q and Conrad A 1997 A review of finite element open boundary techniques for static and quasi-static electromagnetic field problems *IEEE Trans. Magn.* **33** 663–76
Chou St Y 1997 Patterned magnetic nanostructures and quantized magnetic disks *IEEE Trans. Magn.* **85** 652–70
Coffey W T, Crothers D S F, Dormann J L, Kalmykov Yu P, Kennedy E C and Wernsdorfer W 1998 *Phys. Rev. Lett.* **80** 5655–8
Cole J B 1998 Generalized nonstandard finite differences and physical applications *Comput. Phys.* **12** 82–7
Coehoorn R, Mooij D B and Waard C D E 1989 Meltspun permanent magnet materials containing Fe_3B as the main phase *J. Magn. Magn. Mater.* **80** 101–7
Davies H A 1996 Nanocrystalline exchange-enhanced hard magnetic alloys *J. Magn. Magn. Mater.* **158** 11–14
DellaTorre E 1986 Magnetization calculation of fine particles *IEEE Trans. Magn.* **22** 484–9
Demerdash N A and Wang R 1990 Theoretical and numerical difficulties in 3D vector potential methods in finite element magnetostatic computations *IEEE Trans. Magn.* **26** 1656–8
Donahue M J and McMichael R D 1997 Exchange energy representations in computational micromagnetics *Physica* B **233** 272–8
Fabian K, Kirchner A, Williams W, Heider F, Leibi T and Hubert A 1996 Three-dimensional micromagnetic calculations for magnetite using FFT *Geophys. J. Int.* **124** 89–104
Fidler J 1998 *Rare Earth Intermetallic Magnets (Inst. Phys. Conf. Ser. 152 Section G: Magnetic Materials)* pp 805–13
Fidler J, Skalicky P and Rothwarf F 1983 High resolution electron microscope study of $Sm(Co, Fe, Cu, Zr)_{7.5}$ magnets *IEEE-Trans. Magn.* **19** 2041–3
Fischer R and Kronmüller H 1998 Importance of ideal grain boundaries of high remanent composite permanent magnets *J. Appl. Phys.* **83** 3271–5
Fischer R, Leineweber T and Kronmüller H 1998 Fundamental magnetization processes in nanoscaled composite permanent magnets *Phys. Rev.* B **57** 10 723–32
Fredkin D R and Koehler T R 1990 Hybrid method for computing demagnetizing fields *IEEE Trans. Magn.* **26** 415–17
Frei E H, Strikman S and Treves D 1957 Critical size and nucleation field of ideal ferromagnetic particles *Phys. Rev.* **106** 446–55
Fukunaga H and Inoue H 1992 Effect of intergrain exchange interaction on magnetic properties in Nd–Fe–B magnets *Japan. J. Appl. Phys.* **31** 1347–52
Gabay A M, Lileev A S and Menushenkov V P 1992 Simulation of intergranular interaction in sintered magnets *J. Magn. Magn. Mater.* **109** 213–20
Gadbois J, Zhu J G, Vavra W and Hurst A 1998 The effect of end and edge shape on the performance of pseudo-spin valve memories *IEEE Trans. Magn.* **34** 1066–8
Garanin D A 1997 Fokker–Planck and Landau–Lifshitz–Bloch equations for classical ferromagnets *Phys. Rev.* B **55** 3050–7
Gardiner C W 1985 *Handbook of Stochastic Methods* (Berlin: Springer)
Gibbons M R, Parker G, Cerjan C and Hewett D W 1999 Finite difference micromagnetic simulation with self-consistent currents and smooth surfaces *Physica* B **275** 11–16
Gilbert T L 1955 A Lagrangian formulation of gyromagnetic equation of the magnetization field *Phys. Rev.* **100** 1243

Gill P E, Murray W and Wright M H 1993 *Practical Optimization* (London: Academic)
Grossmann C and Roos H-G 1994 *Numerik partieller Differentialgleichungen* 2nd edn (Stuttgart: Teubner)
Hadjipanayis G C and Gong W 1988 Magnetic hysteresis in melt-spun Nd–Pe–Al–B–Si alloys with high remanence *J. Appl. Phys.* **64** 5559–61
Hernando A, Navarro I and Gonzáles J M 1992 On the role of intergranular exchange coupling in the magnetization process of permanent magnet materials *Europhys. Lett.* **20** 175–80
Hertel R and Kronmüller H 1998 Adaptive finite element mesh refinement techniques in three-dimensional micromagnetic modelling *IEEE Trans. Magn.* **34** 3922–30
Herzer G 1989 Grain size dependence of coercivity and permeability in nanocrystalline ferromagnets *IEEE Trans. Magn.* **25** 3327–9
Hindmarsh A C and Petzold L R 1995 Algorithms and software for ordinary differential equations, part II: higher-order methods and software packages *Comput. Phys.* **9** 148–55
Hinzke D and Nowak U 1999 Magnetization switching in a Heisenberg model for small ferromagnetic particles *Phys. Rev.* B **58** 265–72
Inaba N, Uesaka Y, Nakamura A, Futamoto M, Sugita Y and Narishige S 1997 Damping constants of Co–Cr–Ta and Co–Cr–Pt thin films *IEEE Trans. Magn.* **33** 2989–92
Jackson J D 1982 *Elektrodynamik und Relativitätstheorie* (Berlin: de Gruyter)
Kanekiyo H, Uehara M and Hirosawa S 1993 Microstructure and magnetic properties of high-remanence $Nd_5Fe_{14.5}Co_5B_{19.5}M$ (M = Al, Si, Ga, Ag, Au) rapidly solidified and crystallized alloys for resin-bonded magnets *IEEE Trans. Magn.* **29** 2863–5
Khebir A, Kouki A B and Mittra R 1990 Asymptotic boundary for finite element analysis of three-dimensional transmission line discontinuities *IEEE Trans. Microwave Theory Techniques* **38** 1427–31
Kikuchi R 1956 On the minimum of magnetization reversal time *J. Appl. Phys.* **27** 1352–7
Kim A S, Camp F E and Stadelmaier H H 1994 Relation of remanence and coercivity of Nd, (Dy)–Fe, (Co)–B sintered permanent magnets to crystallite orientation *J. Appl. Phys.* **76** 6265–7
Kirk K J, Chapman J N and Wilkinson C D W 199 Lorentz microscopy of small magnetic structures *J. Appl. Phys.* **785** 5237–42
Kneller E P 1991 The exchange-spring material: a new material principle for permanent magnets *IEEE Trans. Magn.* **27** 3588–600
Koch R H, Deak J G, Abraham D W, Trouilloud P L, Altman R A, Lu Y, Gallagher W J, Scheuerlein R E, Roche K P and Parkin S S P 1998 Magnetization reversal in micron-sized magnetic thin films *Phys. Rev. Lett.* **81** 4512–15
Koehler T R 1997 Hybrid FEM-BEM method for fast micromagnetic calculations *Physica* B **233** 302–7
Koehler T R and Fredkin D R 1992 Finite element methods for micromagnetics *IEEE Trans. Magn.* **28** 1239–44
Kuma J, Kitajima N, Kanai Y and Fukunaga H 1998 Maximum energy product of isotropic Nd–Fe–B-based nanocomposite magnets *J. Appl. Phys.* **83** 6623–5
Landau L and Lifshitz E 1935 On the theory of magnetic permeability in ferromagnetic bodies *Physik. Z. Sowjetunion* **8** 153–69
Leineweber T and Kronmüller H 1997 Micromagnetic examination of exchange coupled ferromagnetic nanolayers *J. Magn. Magn. Mater.* **176** 145–54
——1999 Dynamics of magnetization states *J. Magn. Magn. Mater.* **192** 575–90
Lewis D and Della Torre E 1997 Identification of stiff modes in micromagnetic problems *IEEE Trans. Magn.* **33** 1596–9
Liu S, Yang J, Doyle G, Kuhl G E, Chen C, Walmer M and Walmer M 199 New sintered high temperature Sm–Co based permanent magnet materials *IEEE Trans. Magn.* **35** 3325–7

Lyberatos A, Berkov D V and Chantrell R W 1993 A method for the numerical simulation of the thermal magnetization fluctuations in micromagnetics *J. Phys.: Condens. Matter* **5** 8911–20

Marsal D 1989 *Finite Differenzen und Elemente numerische Lsung von Variationsproblemen und partiellen Differential gleichungen* (Berlin: Springer)

McCallum R W, Kadin A M, Clemente G B and Keem J E 1987 High performance isotropic permanent magnets based on Nd–Fe–B *J. Appl. Phys.* **61** 3577–9

McCormick P O, Miao W F, Smith P A, Ding J and Street R 1998 Mechanically alloyed nanocomposite magnets *J. Appl. Phys.* **83** 6256–61

Miles J J and Middleton B K 1990 The role of microstructure in micromagnetic models of longitudinal thin film magnetic media *IEEE Trans. Magn.* **26** 2137–9

Nakatani Y, Uesaka Y and Hayashi N 1989 Direct solution of the Landau–Lifshitz–Gilbert equation for micromagnetics *Japan. J. Appl. Phys.* **28** 2485–507

Nakatani Y, Uesaka Y, Hayashi N and Fukushima H 1997 Computer simulation of thermal fluctuation of fine particle magnetization based on Langevin equation *J. Magn. Magn. Mater.* **168** 347–51

Navarro I, Pulido E, Crespo P and Hernando A 1993 Effect of the hard magnetic inclusion on the macroscopic anisotropy of nanocrystalline magnetic materials *J. Appl. Phys.* **73** 6525–7

Nowak U, Chantrell R and Kennedy E C 2000 Monte Carlo simulation with time step quantification in terms of Langevin dynamics *Phys. Rev. Lett.* **84** 163–6

Nowak U and Hinzke D 1999 Magnetization switching in small ferromagnetic particles: nucleation and coherent rotation *J. Appl. Phys.* **85** 4337–9

Opheusden J H J van and Reuvekamp E M C M 19990 Computer simulation of a thin magnetic film with vertical anisotropy *J. Magn. Magn. Mater.* **88** 247–59

Oti J O 1993 A micromagnetic model of dual-layer magnetic recording thin films *IEEE Trans. Magn.* **29** 1265–75

Parker G J, Cerjan C and Hewett D W 2000 Embedded curve boundary method for micromagnetic simulations *J. Appl. Phys.* **87** 5514–16

Penman J and Grieve M D 1987 Self adaptive mesh generation technique for the finite element method *IEE Proc.* A **134** 634–50

Preparata F P 1985 *Computational Geometry* (New York: Springer)

Ramesh R and Srikrishna K 1988 Magnetization reversal in nucleation controlled magnets: I Theory *J. Appl. Phys.* **64** 6406–515

Richter H J 1999 Recent advances in the recording physics of thin-film media *J. Phys. D: Appl. Phys.* **32** R147–68

Ridley P H W, Roberts G W, Wongsam M A and Chantrell R W 1999 Finite element modelling of nanoelements *J. Magn. Magn. Mater.* **193** 423–6

Rikvold P A, Tomita H, Miyashita S and Sides S W 1994 Metastable lifetimes in a kinetic Ising model: dependence on field and system size *Phys. Rev.* E **49** 5080–90

Russek S E, Oti J O, Kaka S and Chen E Y 1999 High speed characterization of submicrometer giant magnetoresistive devices *J. Appl. Phys.* **85** 4773–5

Sagawa M, Fujimura S, Togawa N, Yamamoto H and Matsuura Y 1984 New material for permanent magnets on a base of Nd and Fe *J. Appl. Phys.* **55** 2083–7

Schabes M E 1991 Micromagnetic theory of non-uniform magnetization processes in magnetic recording particles *J. Magn. Magn. Mater.* **95** 249–88

Schabes M E and Aharoni A 1987 Magnetostatic interaction fields for a three-dimensional array of ferromagnetic cubes *IEEE Trans. Magn.* **23** 3882–8

Schabes M E and Bertram H N 1988 Magnetization processes in ferromagnetic cubes *J. Appl. Phys.* **64** 1347–57

Schmidts H F, Martinek G and Kronmüller H 1992 Recent progress in the interpretation of nucleation fields in hard magnetic particles *J. Magn. Magn. Mater.* **104–7** 1119–20

Scholz W, Schrefl T and Fidler J 1999 Mesh refinement in FE-micromagnetics for multi-domain $Nd_2Fe_{14}B$ particles *J. Magn. Magn. Mater.* **196–7** 933–4

Scholz W, Schrefl T and Fidler J 2000 Micromagnetic simulation of thermally activated switching in fine particles *J. Magn. Magn. Mater.* at press

Schrefl T 1999a Finite elements in numerical micromagnetics: part I: granular hard magnets *J. Magn. Magn. Mater.* **207** 45–65

Schrefl T and Fidler J 1992 Numerical simulation of magnetization reversal in hard magnetic materials using a finite element method *J. Magn. Magn. Mater.* **111** 105–14

——1998 Modelling of exchange spring permanent magnets *J. Magn. Magn. Mater.* **177–81** 970–5

——1999b Finite element modelling of nanocomposite magnets *IEEE Trans. Magn.* **35** 3223–8

Schrefl T, Fidler J, Kirk K J and Chapman J N 1997c Domain structures and switching mechanisms in patterned magnetic elements *J. Magn. Magn. Mater.* **175** 193–204

——1997b A higher order FEM-BEM method for the calculation of domain processes in magnetic nano-elements *IEEE Trans. Magn.* **33** 4182–4

——1999c Simulation of magnetization reversal in polycrystalline patterned Co-elements *J. Appl. Phys.* **85** 6169–71

Schrefl T, Fidler J and Kronmüller H 1994a Remanence and coercivity in isotropic nanocrystalline permanent magnets *Phys. Rev.* B **49** 6100–10

Schrefl T, Fischer R, Fidler J and Kronmüller H 1994b Two- and three-dimensional calculation of remanence enhancement of rare-earth based composite magnets *J. Appl. Phys.* **76** 7053–8

Schrefl T, Roitner H and Fidler J 1997a Dynamic micromagnetics of nanocomposite NdFeB magnets *J. Appl. Phys.* **81** 5567–9

Silvester P P and Ferrari R 1983 *Finite Elements for Electrical Engineers* (Cambridge: Cambridge University Press)

Skomski R and Coey J M D 19993 Giant energy product in nanostructured two-phase magnets *Phys. Rev.* B **48** 15 812–16

Sommeijer B P, Shampine L F and Venwer J G 1998 RKC: an explicit solver for parabolic PDEs *J. Comput. Appl. Math.* **66** 315–26

Spratt G W D, Uesaka Y, Nakatani Y and Hayashi N 19991 Two interacting cubic particles: effect of placement on switching field and magnetization reversal mechanism *IEEE Trans. Magn.* **27** 4790–2

Stoner E C and Wohlfarth E P 1948 A mechanism of magnetic hysteresis in heterogeneous alloys *Phil. Trans. R Soc.* **240** 599–642

Streibl B, Fidler J and Schrefl T 2000 Domain wall pinning in high temperature $Sm(Co, Fe, Cu, Zr)_{7-9}$ magnets *J. Appl. Phys.* **87** 4765–7

Suess D, Schrefl T and Fidler J 2000 Micromagnetic simulation of high energy density permanent magnets *IEEE Trans. Magn.* at press

Suess D, Schrefl T, Fidler J and Chapman J N 1999 Micromagnetic simulation of the long-range interaction between NiFe nano-elements using BE-method *J. Magn. Magn. Mater.* **196–197** 617–19

Tako K M, Schrefl T, Wongsam M A and Chantrell R W 1997 Finite element micromagnetic simulations with adaptive mesh refinement *J. Appl. Phys.* **81** 4082–4

Tang W, Zhang Y and Hadjipanayis G C 2000 Effect of Zr on the microstructure and magnetic properties of $Sm(Co, Fe, Cu, Zr)_{8.5}$ magnets *J. Appl. Phys.* **87** 399–403

Victora R H 1988 Micromagnetic predictions for barium ferrite particles *J. Appl. Phys.* **63** 3423–8

Vos M J, Brott R L, Zhu J G and Carlson L W 19993 Computed hysteresis behaviour and interaction effects in spheroidal particle assemblies *IEEE Trans. Magn.* **29** 3652–7

Weller D and Moser A 1999 Thermal effect limits in

ultrahigh-density magnetic recording *IEEE Trans. Magn.* **35** 4423–39

Wernsdorfer W *et al* 1997 Mesoscopic effects in magnetism: sub-micron to nanometre size single particle measurements *J. Appl. Phys.* **81** 5543–5

Wongsam M A and Chantrell R W 2000 Low temperature spin–spin contributions to Landau–Lifshitz–Gilbert damping *Phys. Rev.* B at press

Yan Y D and Della Torre E 1988 Reversal modes in fine particles *J. Physique Coll.* C8 **49** 1813–14

Yang B and Fredkin D R 1996 Dynamical micromagnetics of a ferromagnetic particle: numerical studies *J. Appl. Phys.* **79** 5755–7

Yang B and Fredkin D R 1998 Dynamical micromagnetics by finite element method *IEEE Trans. Magn.* **43** 3842–52

Yuan S W and Bertram H N 1992 Fast adaptive algorithms for micromagnetics *IEEE Trans. Magn.* **28** 2031–6

Zhang K and Fredkin D R 1999 Stochastic dynamic micromagnetic study of fine particles *J. Appl. Phys.* **85** 5208–10

Zhu J G 1992 Modelling of multilayer thin film recording media *IEEE Trans. Magn.* **28** 3267–9

——1995 Micromagnetic modelling: theory and application in magnetic thin films *MRS Bull.* **20** 49–54

Zhu J G and Bertram H N 1988 Micromagnetic study of thin metallic films *J. Appl. Phys.* **63** 3248–53